

# Quasinormal modes of Proca and Maxwell fields in $d$ -dimensional Schwarzschild-AdS black holes

David C. Lopes,<sup>1,\*</sup> Tiago V. Fernandes,<sup>2,†</sup> and José P. S. Lemos<sup>3,‡</sup>

<sup>1</sup>*Centre for Astrophysics Research, Department of Physics, Astronomy and Mathematics, University of Hertfordshire, Hatfield AL10 9AB, United Kingdom, & Centro de Astrofísica e Gravitação - CENTRA, Departamento de Física, Instituto Superior Técnico - IST, Universidade de Lisboa - UL, Avenida Rovisco Pais 1, 1049-001 Lisboa, Portugal*

<sup>2</sup>*Centro de Astrofísica e Gravitação - CENTRA, Departamento de Física, Instituto Superior Técnico - IST, Universidade de Lisboa - UL, Avenida Rovisco Pais 1, 1049-001 Lisboa, Portugal*

<sup>3</sup>*Center for Astrophysics and Space Science, School of Mathematical and Physical Sciences, Macquarie University, Sydney, New South Wales 2109, Australia, & Centro de Astrofísica e Gravitação - CENTRA, Departamento de Física, Instituto Superior Técnico - IST, Universidade de Lisboa - UL, Av. Rovisco Pais 1, 1049-001 Lisboa, Portugal*

Proca and Maxwell fields in  $d$ -dimensional Schwarzschild black holes with anti-de Sitter (AdS) asymptotics are investigated through their linear perturbations and associated quasinormal modes (QNMs) with Dirichlet boundary conditions at infinity. We begin by reviewing how the Proca field equations in  $d$ -dimensional spherically symmetric spacetimes reduce to three radial wave-like equations, one fully decoupled equation and two mutually coupled equations. We also demonstrate explicitly how the Maxwell equations emerge from the zero-mass limit of the Proca system. Several analytical properties of the corresponding QNM spectrum are examined. To compute the QNM frequencies, we employ two complementary numerical methods particularly suited to asymptotically AdS spacetimes. Using these techniques, we determine the QNMs modes of Proca field perturbations in 4, 5, 6, and 7-dimensional Schwarzschild-AdS backgrounds. As a new result, we find numerically that scalar-type Maxwell perturbations in large  $d \geq 5$  Schwarzschild-AdS black holes exhibit purely imaginary low-frequency modes, analogous to those found in vector-type gravitational perturbations. The presence of such modes is especially relevant within the AdS/CFT correspondence, as they correspond to the linearized hydrodynamic regime in the dual conformal field theory. We further analyze the influence of the Proca mass on the QNM spectrum, also emphasizing how Maxwell modes are recovered in the massless limit. The dependence of the spectrum on the black hole radius is explored. In addition, analytic expressions for the QNM frequencies of vector-type and monopole Proca perturbations, as well as Maxwell modes, are derived for small  $d$ -dimensional Schwarzschild-AdS black holes by matching asymptotic expansions using an intermediate region. These analytic results show good agreement with the numerical findings, confirming, in particular, the existence of purely imaginary low-frequency scalar-type Maxwell modes in large  $d \geq 5$  Schwarzschild-AdS spacetimes.

## I. INTRODUCTION

An important aspect of analyzing the linear stability of stationary systems involves understanding how these systems respond when subjected to small perturbations. Such analyses are essential for determining whether a system will return to its original state after a slight de-

viation, evolve toward a new equilibrium configuration, or become unstable over time when perturbed from its initial state. In the context of black hole spacetimes, the response to a small external perturbation is typically dominated, at intermediate times, by the quasinormal mode (QNM) ringing phase, during which the perturbations can be described in terms of a discrete, countable set of QNM frequencies and their associated eigenfunctions. These frequencies are generally complex numbers. The real part of the frequency corresponds to the actual oscillation frequency, and the imaginary part determines whether the perturbation decays or grows in time. The

\* david.d.lopes@tecnico.ulisboa.pt

† tiago.vasques.fernandes@tecnico.ulisboa.pt

‡ joselemos@ist.utl.pt

imaginary component of the QNM frequencies, in particular, provides critical information about the linear stability of the perturbed spacetime. Specifically, if all QNMs are damped, which means that their amplitudes decrease in time, the spacetime is considered linearly stable under the class of perturbations being investigated. On the other hand, if any mode exhibits growth with time, it signals an instability within the system. Beyond their role in stability analysis, these modes also carry information about how perturbations evolve in curved spacetimes. They are closely related to observable phenomena, for instance, the gravitational wave signals produced when black holes respond to dynamical perturbations.

To provide an overview on QNMs, we focus in three classes of black hole spacetimes. First, asymptotically flat black hole spacetimes, in which the geometry approaches that of Minkowski space at large distances, representing isolated gravitational systems. Second, asymptotically de Sitter (dS) black hole spacetimes, which describe black holes in universes with a positive cosmological constant. Third, asymptotically anti-de Sitter (AdS) black hole spacetimes, characterized by a negative cosmological constant, which play an important role in several areas of physics, particularly in supergravity, holography, and the AdS/CFT correspondence, where QNMs are closely related to relaxation processes in the dual conformal field theory.

We first turn our attention to black holes in asymptotically flat spacetimes, i.e., black hole spacetime where the cosmological constant is set to zero. The Schwarzschild black hole, as the simplest spherically symmetric solution of general relativity, provided the natural starting point for investigations of black hole stability under linear perturbations. The stability against gravitational perturbations was tested in several early works, notably by Regge and Wheeler, Zerilli, and Vishveshwara [1–3] that laid the basis for the development of black hole perturbation theory. Extending the analysis to Maxwell electromagnetic perturbations, Reissner-Nordström black holes, i.e., spherical black holes with electric charge, were investigated in [4]. It was shown that the equations governing perturbations in such a black hole background could be reduced to a single, wave-like equation, simplifying the analysis. For rotating, uncharged black holes in general relativity, namely Kerr black holes, it was shown in [5] that both electromagnetic and gravitational perturbations can be separated analytically. This work also addressed the stability of rotating black holes and the phenomenon of superradiant scattering. Related to perturbations are the QNMs, i.e., the damped oscillations that dominate the late-time response of black holes to perturbations. The QNMs of the Schwarzschild black hole were computed for the first time in [6], and their interpretation has become central in black hole and gravitational wave physics. A systematic treatment of massless field perturbations with various spin values, including scalar, electromagnetic, and gravitational, was provided by Chandrasekhar [7], further developing the framework

of linear perturbation theory in black hole spacetimes. The situation becomes more complicated in the presence of massive vector fields, known as Proca fields. Unlike the massless case, where gauge freedom simplifies the analysis, the Proca field’s mass term explicitly breaks gauge invariance. This breaking introduces an additional propagating degree of freedom, leading to coupling between the different components of the field. As a result, the perturbation equations become more intricate and, in general, do not decouple for arbitrary values of the angular momentum quantum number, even in the static black hole background [8]. This complexity poses challenges to attempts at an analytical treatment and obliges to use numerical methods for further understanding. For scalar massive fields, an initial treatment can be found in [9]. A comprehensive review of the subject, encompassing not only QNMs of black holes but also those of relativistic stars, is provided in [10], where the theoretical framework is discussed and applications are given. The case of massless vector fields, specifically Maxwell fields, and their perturbations on static black hole spacetimes was explored in [11], and for Proca fields it was demonstrated in [12] that monopole, i.e., zero angular momentum, Proca perturbations can be reduced to a decoupled wave-like equation, a simplification that does not extend to perturbations with general angular momentum, where the coupling between different modes persists. Further studies of massive scalar field perturbations were performed in [13, 14], providing insights into their dynamics and into the QNM spectrum. The phenomenon of superradiant instabilities through scalar fields was investigated in [15], which analyzed the conditions under which energy extraction from black holes becomes possible. In another study, Proca field perturbations and their associated QNMs were analyzed in detail in [16], where a comprehensive examination of the spectrum of such massive vector fields in black hole spacetimes was done. Additionally, the behavior of massless vector fields in higher-dimensional,  $d \geq 4$ , black holes was analyzed in [17], where it was shown that the perturbation equations reduce to two decoupled wave-like equations, one governing a scalar-type degree of freedom and the other governing the remaining  $d - 3$  vector-type degrees of freedom. For a more extensive discussion of these topics and further developments, the reader is referred to the review in [18]. In [19], the dynamics of a massive vector, i.e., a Proca field in the 4-dimensional Schwarzschild spacetime was explored, with a particular focus on QNMs and bound states for higher multipole moments. This study marked an advancement in understanding the spectrum of Proca fields in spherically symmetric black hole backgrounds beyond the monopole case. A subsequent and more comprehensive analysis of Proca field perturbations was carried out for  $d$ -dimensional black holes in [20]. There, the authors showed that the field equations can be systematically decomposed into a set of three radial wave-like equations, two coupled equations governing the scalar-type modes of the Proca field, and one fully decoupled equa-

tion describing the  $d - 3$  vector-type degrees of freedom. This decomposition provides a more tractable framework for analyzing the field dynamics, although the coupled nature of the scalar-type sector still presents computational challenges. A further review and discussion of perturbations, particularly in relation to massive fields and their stability properties, is presented in [21]. The case of rotating black holes was tackled in [22, 23], where the behavior of massive Proca fields in the Kerr geometry was studied. These works identified conditions under which superradiant instabilities may arise, contributing to the broader investigation of massive field instabilities in rotating spacetimes. More recent work in [24] extended the analysis to scenarios involving vector fields that are nonminimally coupled to curvature, examining how such couplings influence the QNM spectrum and may modify the stability of black hole solutions. Finally, in [25], superradiant instabilities were investigated in the context of charged regular black holes. This study treated energy extraction mechanisms in regular black hole spacetimes considering both the regularity of the metric and the presence of an electromagnetic field, showing how such features alter the superradiant phenomenon.

We next mention black holes in asymptotically dS spacetimes, i.e., black hole spacetimes where the cosmological constant is set to be positive. The presence of a cosmological horizon in these geometries introduces new features absent in asymptotically flat spacetimes, such as a finite volume between the event and cosmological horizons, and the setting of boundary conditions relevant for the analysis. These differences influence the behavior of QNMs and imply the need for an appropriate treatment. The first analysis of QNMs and the stability of black holes in dS space was carried out in [26], where insights into the characteristic decay of fields in the presence of an event and a cosmological horizon were given. Further developments were achieved in the context of near-extremal dS black holes, where the event and cosmological horizons become nearly coincident, demonstrating that an analytical approach is possible to test the stability of the spacetimes [27]. Other results on the QNMs of Schwarzschild-dS black holes were obtained in [28, 29]. These works employed analytical and numerical techniques to compute the QNM spectra for scalar, electromagnetic, and gravitational perturbations and showed that increasing the cosmological constant lowers the real part of the QNM frequencies and modifies the damping rates. The effects of massive scalar fields propagating in Schwarzschild-dS black hole backgrounds were investigated in [30]. In particular, the interplay between the scalar field mass and the cosmological constant leads to the appearance of an effective potential that alters the stability of the spacetime and the propagation of waves.

Finally, we turn our view onto black holes in asymptotically AdS spacetimes, i.e., black hole spacetimes where the cosmological constant is set to be negative, which the subject of our main interest. The study of QNMs in AdS spacetimes began with the analysis of scalar per-

turbations in Schwarzschild-AdS black holes in [31], followed by investigations of scalar, electromagnetic, and Weyl perturbations in BTZ black holes in [32]. Subsequent work extended the analysis to electromagnetic and gravitational perturbations of Schwarzschild-AdS black holes in [33], and to planar, cylindrical, and toroidal black holes in [34]. Further developments in [35] analyzed Reissner-Nordström-AdS spacetimes and computed its quasinormal modes, and in [36] the QNM spectrum of Schwarzschild-AdS black holes was shown to exhibit distinct asymptotic regimes where frequencies scale with the black hole size and approach evenly spaced patterns determined by the AdS boundary conditions. A general framework for studying perturbations and QNMs in arbitrary spacetime dimensions was developed in [37–39], a method that also encompasses zero and positive cosmological constant cases. The dynamics and wave equations of various fields in AdS spacetimes were analyzed in [40]. Tensorial, i.e., gravitational perturbations of planar black holes were studied in [41], while scalar field perturbations and instabilities in Kerr-AdS spacetimes were reported in [42]. QNMs of AdS black holes in the context of expanding plasmas were explored in [43], and the high-wavelength eikonal regime was examined in [44]. The stability of Reissner-Nordström-AdS black holes in general relativity in four and higher dimensions, was investigated through perturbation analysis in [45, 46]. Finally, a broad spectrum of perturbations, including Maxwell fields, and the emergence of superradiant instabilities in AdS black hole spacetimes were studied in [47, 48]. Proca field perturbations in extremal and near-extremal static black hole spacetimes were investigated in [49] and the QNMs of Proca fields in four-dimensional Schwarzschild-AdS spacetime were further analyzed in [50], with a focus on the decoupling of the degrees of freedom. Normal modes of Proca perturbations in pure AdS spacetime were explored in [51]. QNMs in cylindrical AdS black holes were further studied in [52], while a comprehensive analysis of various boundary conditions in AdS black hole backgrounds was presented in [53]. In [54], the normal modes of Proca fields in pure AdS spacetimes for general spacetime dimensions  $d \geq 4$  were derived. This work showed that the Proca equations reduce to a system of three radial wave-like equations, namely, two coupled equations describing the scalar-type modes and a single decoupled equation governing the  $d - 3$  vector-type mode. Finally, the QNM spectrum of a Proca field in five-dimensional Schwarzschild-AdS spacetime was obtained using the isomonodromy method in [55].

Taken together, previous studies, some of which we mentioned above, have built a consistent picture of black hole perturbations in asymptotically flat, de Sitter, and Anti-de Sitter spacetimes. This provides an effective framework where different boundary conditions and geometric setups can be compared on the same footing. In particular, the QNMs in black hole spacetimes play an important role in describing how perturbations evolve and decay in time and how the spacetime reacts to ex-

ternal and internal excitations. These results have been important for understanding several physical and observational aspects, including stability, energy dissipation, and gravitational wave emission. In the AdS case, they also connect naturally with holographic descriptions. In this work, we focus on QNMs of Proca fields, specifically, in massive vector perturbations, in higher-dimensional, spherically symmetric, asymptotically AdS black hole spacetimes. The field's mass and the presence of extra dimensions can affect the spectrum. Our main motivation is to better understand how mass and spin affect the QNM spectrum and to explore the effect of higher dimensions on the dynamics of black hole spacetimes. Let us consider these topics more carefully. First, higher-dimensional spacetimes play an important role in various theoretical settings, including string theory and braneworld scenarios, which allow for extra spatial dimensions beyond the usual four. These approaches have motivated the study of new black hole solutions in higher dimensions [56], which can show a different behavior from the four-dimensional ones. Second, asymptotically AdS spacetimes are interesting not just from a theoretical point of view but also mathematically. They show up in theories like supergravity and also play a role in the AdS/CFT correspondence, which links gravity in AdS space to a conformal field theory on its boundary. For a more detailed discussion physical and mathematical significance of AdS spacetimes, see [57]. Third, the study of massive spin-1 fields is highly relevant both within and beyond the standard model of particle physics. In particular, massive vector fields, such as the Proca field, have gained increasing interest in the context of dark matter models, including scenarios involving light bosonic candidates such as axions and fuzzy cold dark matter. These fields interact predominantly through gravity, making it essential to understand their behavior in curved spacetime, especially in regions near the horizon of black holes. For an overview and classification of dark matter candidates, see [58]. Fourth and finally, given the growing theoretical and phenomenological interest in massive vector fields, a comprehensive study of the QNMs associated with Proca perturbations in higher-dimensional asymptotically AdS black hole spacetimes is both opportune and appropriate. Such a study is essentially absent from the literature, leaving a gap that we attempt to fill here. Therefore, our research is focused on providing a systematic and detailed investigation of QNMs of Proca fields in higher-dimensional, spherically symmetric AdS black holes, dealing with the QNM dynamical properties and the stability behavior in these geometries.

The paper is organized as follows. In Sec. II, we introduce the equations describing a Proca field minimally coupled to a general relativistic  $d$ -dimensional curved spacetime. In Sec. III, we review how the Proca field equations in  $d$ -dimensional spherically symmetric spacetimes reduce to three radial wave-like equations, two equations coupled between themselves, and another completely decoupled. We also carefully study how the

Maxwell equations arise from the zero mass limit of the Proca equations. In Sec. IV, we investigate some analytical properties of the QNMs of Proca and Maxwell field perturbations. In Sec. V, we detail the numerical techniques employed to compute the QNM frequencies. Two methods are used. The shooting method, which involves numerically integrating the perturbation equations. This approach is well-established in the literature, particularly for asymptotically flat spacetimes, see, e.g., [6, 18, 21], and has also been adapted for asymptotically AdS backgrounds [45]. And the Horowitz-Hubeny numerical method, specifically designed for asymptotically AdS spacetimes, which is known for its efficiency and reliability in this context, see [31, 50]. These complementary methods allow us to determine with accuracy the QNM spectra across different spacetime geometry parameters. In Sec. VI, we compute the Proca and Maxwell QNM frequencies in 4, 5, 6, 7-dimensional Schwarzschild-AdS spacetime. In particular, we find numerically that scalar-type Maxwell perturbations in  $d \geq 5$  large Schwarzschild-AdS spacetimes exhibit purely imaginary low frequency modes, which are similar to those found for vector-type gravitational perturbations in [33, 34, 36, 41]. The existence of such modes is relevant in the AdS/CFT correspondence, as these correspond to the linearized hydrodynamic regime in the CFT side [43, 44]. Furthermore, the effect of the mass of the Proca field on the QNMs is studied, with an emphasis on how the Maxwell modes can be obtained from the massless limit of the Proca modes. Additionally, we investigate the dependence of the QNMs on the black hole radius. In Sec. VII, we obtain analytic expressions for the QNMs of vector-type and monopole Proca perturbations, as well as the Maxwell modes, for small  $d$ -dimensional Schwarzschild-AdS black holes. We do this by matching asymptotic expansions of the solution in an intermediate region, see e.g., [15, 19] for asymptotically flat spacetimes and [42, 46, 47] for asymptotically AdS. The analytical results are compared with the numerical ones, and the comparison shows good agreement in the relevant regimes. In Sec. VIII, we conclude emphasizing that we have obtained the QNMs of Proca and Maxwell perturbations in higher-dimensional Schwarzschild-AdS spacetime with Dirichlet boundary conditions, thus generalizing the study made in [50].

We use Planck units throughout the paper, i.e.,  $\hbar = 1$ ,  $G = 1$ , and  $c = 1$ . Moreover, spacetime indices are denoted by Greek letters, e.g.,  $\mu, \nu$ , run from 0 to  $d - 1$ , where 0 is the time index, and 1 to  $d - 1$  specify the spatial indices.

## II. PROCA AND MAXWELL FIELDS IN CURVED SPACETIME

The dynamics of a Proca field minimally coupled to a  $d$ -dimensional gravitational background with negative cosmological constant is encoded in the Einstein-Proca action,  $S = S_E + S_P$ , where  $S_E = \frac{1}{16\pi} \int d^d x \sqrt{-g} (R - 2\Lambda)$  is the Einstein action,  $S_P = - \int d^d x \sqrt{-g} (\frac{1}{2} \mu^2 A_\mu A^\mu + \frac{1}{4} F_{\mu\nu} F^{\mu\nu})$  is the Proca field action,  $g$  is the determinant of the metric  $g_{\mu\nu}$ ,  $R = R_{\mu\nu} g^{\mu\nu}$  is the Ricci scalar, defined as the trace of the Ricci tensor  $R_{\mu\nu}$  calculated in terms of the metric itself and its first and second derivatives,  $\Lambda = -\frac{(d-1)(d-2)}{2l^2}$  is the cosmological constant, with  $l$  being the characteristic AdS length,  $A_\mu$  is the Proca field with mass  $\mu$ , and  $F_{\mu\nu} \equiv \nabla_\mu A_\nu - \nabla_\nu A_\mu$  is the Proca field strength, with  $\nabla_\mu$  representing the covariant derivative with respect to the  $x^\mu$  coordinate. For zero field mass,  $\mu = 0$ , the action  $S$  turns into the Einstein-Maxwell action. The field equations for the metric and for the Proca field are obtained by applying the variational principle to the action  $S$ . Variation of the action  $S$  with respect to the metric gives the Einstein equation,

$$G_{\mu\nu} - \frac{(d-1)(d-2)}{2l^2} g_{\mu\nu} = 8\pi T_{\mu\nu},$$

$$T_{\mu\nu} \equiv g^{\alpha\beta} F_{\mu\alpha} F_{\nu\beta} + \mu^2 A_\mu A_\nu - g_{\mu\nu} \left( \frac{1}{4} F_{\alpha\beta} F^{\alpha\beta} + \frac{\mu^2}{2} A_\alpha A^\alpha \right), \quad (1)$$

where  $G_{\mu\nu} = R_{\mu\nu} - \frac{1}{2} g_{\mu\nu} R$  is the Einstein tensor and  $T_{\mu\nu}$  is the Proca stress-energy tensor. Moreover, the Einstein tensor obeys the Bianchi identity  $\nabla^\nu G_{\mu\nu} = 0$ , which in turn implies the conservation law for  $T_{\mu\nu}$ , i.e.,  $\nabla^\nu T_{\mu\nu} = 0$ . The Proca field equation can be obtained by varying the action  $S$  with respect to the Proca field  $A_\mu$  to give

$$\nabla_\nu F^{\mu\nu} + \mu^2 A^\mu = 0. \quad (2)$$

Due to  $F_{\mu\nu}$  being an antisymmetric tensor, one can calculate the divergence of the Proca field equation, to obtain an equation for  $A_\mu$ , i.e.,  $\nabla^\mu A_\mu = 0$ . For  $\mu^2 \neq 0$  this equation is the Bianchi identity for the field  $A_\mu$ . In this nonzero field mass case,  $A_\mu$  is a physical field with only  $d-1$  dynamical degrees of freedom, as one component of the field can always be determined from the others precisely by the Proca Bianchi identity  $\nabla^\mu A_\mu = 0$ . For  $\mu^2 = 0$ ,  $A_\mu$  reduces to the Maxwell field obeying the field equation  $\nabla_\nu F^{\mu\nu} = 0$ , and the Bianchi identity  $\nabla^\mu A_\mu = 0$  ceases to exist, as it no longer follows from the field equation. In turn,  $A_\mu$  becomes invariant under the gauge transformation  $A^\mu \rightarrow A^\mu + \partial^\mu h$ , where  $h$  is an arbitrary scalar field, and what was the Bianchi identity for  $A_\mu$  becomes the Lorenz gauge condition of the Maxwell field, which does not completely fix the gauge, as it is still gauge-invariant if  $\nabla_\mu \nabla^\mu h = 0$ , i.e., if  $h$  obeys the massless Klein-Gordon equation. Thus, in the massless case,  $A_\mu$  only has  $d-2$  dynamical degrees of freedom.

The full dynamics of a Proca field propagating in curved spacetime can only be captured by solving Eqs. (1) and (2) simultaneously for both  $g_{\mu\nu}$  and  $A_\mu$ , taking into account the Proca stress-energy tensor  $T_{\mu\nu}$  defined in Eq. (1). Here, we will consider the Schwarzschild-AdS solution of the vacuum Einstein field equations with negative cosmological constant and the trivial  $A_\mu = 0$  solution, and then take into account linear perturbations of the Proca field around  $A_\mu = 0$ . Since  $T_{\mu\nu}$  defined in Eq. (1) is of second order in  $A_\mu$ , perturbations in the Proca field do not induce a curvature perturbation on  $g_{\mu\nu}$  in first order. Thus, in first order, the metric is still described by the background metric as a solution to vacuum Einstein field equations in Eq. (1) with  $A_\mu = 0$ , while the perturbations of the Proca field are described by the Proca field equations Eq. (2), with a fixed background metric. In the same way, the Maxwell field can be treated as a perturbation on a background that is not itself perturbed, either by taking the massless limit of the Proca field with care or by considering the Maxwell field from the start.

## III. LINEAR PROCA AND MAXWELL FIELD PERTURBATIONS IN SCHWARZSCHILD-ADS

### A. Proca equations in spherically symmetric backgrounds: The radial equations in Schwarzschild-AdS

#### 1. Proca equations in spherically symmetric backgrounds

We are interested in solving Eq. (2) in a  $d$ -dimensional Schwarzschild-AdS spacetime, which is a static spherically symmetric vacuum solution to the Einstein field equations with negative cosmological constant described by Eq. (1). The coordinates  $x^\mu$  used are the time coordinate  $x^0 \equiv t$ , the radial coordinate  $x^1 \equiv r$ , and the angular polar coordinates  $x^i \equiv \theta^i$ , with  $i = 2, 3, \dots, d-1$ . For a metric  $g_{\mu\nu}$ , the line element  $ds^2$  is generically given by  $ds^2 = g_{\mu\nu} dx^\mu dx^\nu$ , and for  $d$ -dimensional Schwarzschild-AdS spacetime the line element in Schwarzschild spherical coordinates is given by

$$ds^2 = -f(r) dt^2 + \frac{dr^2}{f(r)} + r^2 d\Omega_{d-2}^2, \quad (3)$$

where  $f(r)$  is

$$f(r) = 1 + \frac{r^2}{l^2} - \left( 1 + \frac{r_h^2}{l^2} \right) \left( \frac{r^2}{l^2} \right)^{d-3}, \quad (4)$$

$d\Omega_{d-2}^2$  is the line element of the  $(d-2)$ -sphere in polar coordinates  $\theta^i$ , with  $i = 2, 3, \dots, d-1$ , given by  $d\Omega_{d-2}^2 = (d\theta^2)^2 + \sum_{i=3}^{d-1} \prod_{k=2}^{i-1} \sin^2(\theta^k) (d\theta^i)^2$ , and  $r_h$  is the event horizon radius, the only positive root of  $f(r)$ .

In spherically symmetric spacetimes, the Proca equations Eq. (2) reduce to a set of radial wave-like equations

[20, 49, 54], using the decomposition given in [37]. This decomposition of the Proca field consists in expanding its components according to their tensorial behavior on the  $(d-2)$ -sphere, using the appropriate spherical harmonics. More concretely, we assume the following ansatz for the Proca field [54]

$$\begin{aligned} A_\mu dx^\mu &= r^{1-\frac{d}{2}} \sum_{\vec{k}_s} \left( u_{0\vec{k}_s}(t, r) dt + \frac{u_{1\vec{k}_s}(t, r)}{f(r)} dr \right) Y_{\vec{k}_s} \\ &+ r^{1-\frac{d}{2}} \sum_{\vec{k}_s} \left[ \frac{r u_{2\vec{k}_s}(t, r)}{\ell(\ell+d-3)} \hat{\nabla}_i Y_{\vec{k}_s} d\theta^i \right] \\ &+ r^{2-\frac{d}{2}} \sum_{\vec{k}_v} u_{3\vec{k}_v}(t, r) Y_{\vec{k}_v, i} d\theta^i, \end{aligned} \quad (5)$$

where  $Y_{\vec{k}_s}$  and  $Y_{\vec{k}_v, i}$  are, respectively, the scalar and vector spherical harmonics on the  $(d-2)$ -sphere,  $\hat{\nabla}_i$  denotes the covariant derivative associated to the  $(d-2)$ -sphere, the functions  $u_{0\vec{k}_s}$ ,  $u_{1\vec{k}_s}$ , and  $u_{2\vec{k}_s}$  are the functions that describe the time and radial dependence of the scalar sector of the Proca field, while  $u_{3\vec{k}_v}$  describes the time and radial dependence of the vector sector of the Proca field, and  $\vec{k}_s, \vec{k}_v$  in the subscript are vectors containing the angular momentum number,  $\ell$ , and the  $d-3$  azimuthal numbers associated to each harmonic. Substituting Eq. (5) in Eq. (2), the Proca field equations completely separate in two different sectors, namely, the scalar-type sector, whose components behave as scalars on the sphere, covering two degrees of freedom of the Proca field, and the vector-type sector, whose components behave as vectors on the sphere, covering the other  $d-3$  degrees of freedom of the Proca field.

The scalar-type modes of the Proca field perturbations are coupled, and are described by the following system of wave-like equations for each harmonic vector  $\vec{k}_s$

$$\begin{aligned} \mathcal{D}_\ell u_0 + \frac{(d-4)f}{r^2} \left( 1 - f + \frac{r f'}{2} \right) u_0 \\ + f' (\partial_t u_1 - \partial_{r_*} u_0) = 0, \end{aligned} \quad (6)$$

$$\begin{aligned} \mathcal{D}_\ell u_1 + f \left( \frac{d-4}{r^2} - \frac{2(d-3)}{r^2} f + \frac{(d-3)}{r} f' \right) u_1 \\ - \frac{f}{r} \left( f' - \frac{2f}{r} \right) u_2 = 0, \end{aligned} \quad (7)$$

$$\mathcal{D}_\ell u_2 + f \frac{(d-4)}{r^2} u_2 + \frac{2f\ell(\ell+d-3)}{r^2} u_1 = 0, \quad (8)$$

where  $\mathcal{D}_\ell$  is the operator defined by

$$\begin{aligned} \mathcal{D}_\ell = -\partial_t^2 + \partial_{r_*}^2 - \\ f \left( \frac{(\ell+1)(\ell+d-4)}{r^2} + \frac{(d-4)(d-6)}{4r^2} f \right. \\ \left. + \frac{(d-4)}{2r} f' + \mu^2 \right), \end{aligned} \quad (9)$$

with  $dr_*$  being defined through  $dr_* = \frac{dr}{f(r)}$ ,  $\partial_t$  and  $\partial_{r_*}$  denoting partial derivatives in relation to  $t$  and  $r_*$ , respectively, a dash meaning derivative with respect to  $r$ ,

and where we have suppressed the harmonic vectors in the subscript of  $u_0$ ,  $u_1$  and  $u_2$ . The Bianchi identity, for  $A_\mu$ , i.e.,  $\nabla^\mu A_\mu = 0$ , relates the scalar sector functions through

$$\partial_t u_0 - \partial_{r_*} u_1 = \frac{f}{r} \left( \frac{d-2}{2} u_1 - u_2 \right). \quad (10)$$

On the other hand, the vector-type modes are all decoupled and described by the same wave-like equation,

$$\mathcal{D}_\ell u_3 = 0, \quad (11)$$

where we have suppressed the harmonic indices in  $u_3$ .

## 2. Proca radial equations in Schwarzschild-AdS

The QNMs of Proca field perturbations in Schwarzschild-AdS are dynamical solutions of Eqs. (6)-(11) for  $u_0$ ,  $u_1$ ,  $u_2$  and  $u_3$ , with the appropriate boundary conditions specified at the event horizon and at spatial infinity. By disregarding the static solution of  $u_0$  to Eq. (6), one can choose  $u_0$  to be completely determined from  $u_1$  and  $u_2$  through Eq. (10), so that the physical solutions are described solely by Eqs. (7)-(8) for  $u_1$  and  $u_2$ , and by Eq. (11) for  $u_3$ . By further assuming a time dependence of the form

$$u(r, t) = u(r) e^{-i\omega t}, \quad (12)$$

the wave-like equations become Schrödinger-like equations for the mode frequencies  $\omega$ , with associated effective potentials which, alongside with the boundary conditions, determine the dynamics of the perturbations of the Proca field.

For the scalar-type modes, the perturbations are ruled by the coupled system of equations

$$\partial_{r_*}^2 \mathbf{u} + (\omega^2 \mathbf{I} - \mathbf{V}_s) \mathbf{u} = 0, \quad (13)$$

where  $\mathbf{u} = (u_1 \ u_2)^T$ ,  $\mathbf{I}$  is the identity matrix and  $\mathbf{V}_s$  can be read from Eqs. (7) and (8) as

$$\mathbf{V}_s = \begin{pmatrix} V_{s11} & V_{s12} \\ V_{s21} & V_{s22} \end{pmatrix}, \quad (14)$$

with the following components

$$\begin{aligned}
V_{s11} &= f \left( \frac{(d-4)(d-2) + 4\mu^2 l^2}{4l^2} \right. \\
&\quad + \frac{4\ell(\ell+d-3) + d(d-2)}{4r^2} \\
&\quad \left. - \frac{3(d-2)^2}{4r_h^2} \left( 1 + \frac{r_h^2}{l^2} \right) \left( \frac{r_h}{r} \right)^{d-1} \right), \\
V_{s12} &= f \left( -\frac{2}{r^2} + \frac{d-1}{4r_h^2} \left( 1 + \frac{r_h^2}{l^2} \right) \left( \frac{r_h}{r} \right)^{d-1} \right), \\
V_{s21} &= -f \frac{2\ell(\ell+d-3)}{r^2}, \\
V_{s22} &= f \left( \frac{(d-4)(d-2) + 4\mu^2 l^2}{4l^2} \right. \\
&\quad + \frac{4\ell(\ell+d-3) + (d-4)(d-6)}{4r^2} \\
&\quad \left. - \frac{d(d-4)}{4r_h^2} \left( 1 + \frac{r_h^2}{l^2} \right) \left( \frac{r_h}{r} \right)^{d-1} \right). \quad (15)
\end{aligned}$$

The monopole mode,  $\ell = 0$ , is described uniquely by Eq. (7) with  $u_2 = 0$ , and so by the one-dimensional Schrödinger-like with potential  $V_{s11}$ .

For vector-type perturbations, the radial equation in Eq. (11) can be written as

$$\partial_{r_*}^2 u_3 + (\omega^2 - V_v)u_3 = 0, \quad (16)$$

with the potential

$$\begin{aligned}
V_v &= f \left( \frac{(d-4)(d-2) + 4\mu^2 l^2}{4l^2} \right. \\
&\quad + \frac{(2\ell+d-4)(2\ell+d-2)}{4r^2} \\
&\quad \left. + \frac{d(d-4)}{4r_h^2} \left( 1 + \frac{r_h^2}{l^2} \right) \left( \frac{r_h}{r} \right)^{d-1} \right). \quad (17)
\end{aligned}$$

### B. Maxwell equations in spherically symmetric backgrounds: The radial equations in Schwarzschild-AdS

The Maxwell field equations can be obtained by carefully taking the massless limit of the Proca field equations. As explained in Section II, the equations are now invariant under a gauge transformation, and the Maxwell field carries pure gauge degrees of freedom that need to be eliminated.

The scalar-type sector contains pure-gauge degrees of freedom, and one needs to find a suitable gauge-invariant combination of scalar-type variables to describe the unique scalar-type physical degree of freedom. This is achieved by defining the gauge-invariant variable

$$u_{12} = \frac{u_1}{r} - \frac{r^{\frac{d}{2}-2}}{\ell(\ell+d-3)} \partial_{r_*} \left( r^{2-\frac{d}{2}} u_2 \right), \quad (18)$$

which yields the Maxwell equation for the physical scalar-type degree of freedom,

$$\partial_{r_*}^2 u_{12} + (\omega^2 - V_{sm})u_{12} = 0, \quad (19)$$

with

$$\begin{aligned}
V_{sm} &= f \left( \frac{(d-4)(d-6)}{4l^2} \right. \\
&\quad + \frac{(2\ell+d-4)(2\ell+d-2)}{4r^2} \\
&\quad \left. - \frac{(3d-8)(d-4)}{4r_h^2} \left( 1 + \frac{r_h^2}{l^2} \right) \left( \frac{r_h}{r} \right)^{d-1} \right), \quad (20)
\end{aligned}$$

where the subscript m stands for Maxwell to distinguish from the Proca case. In order to understand what happens when taking the massless limit of the Proca scalar-type sector, i.e., to understand Eqs. (18)-(20), it is useful to write Eq. (8) as

$$\mathcal{D}_\ell^{s=0}(ru_2) = -2\ell(\ell+d-3)fu_{12}, \quad (21)$$

where  $\mathcal{D}_\ell^{s=0}$  is the operator ruling the dynamics of a massive scalar field propagating in a spherically symmetric background which is given by [31]

$$\begin{aligned}
\mathcal{D}_\ell^{s=0} &= -\partial_t^2 + \partial_{r_*}^2 \\
&\quad - f \left( \frac{\ell(\ell+d-3)}{r^2} + \frac{(d-2)(d-4)}{4r^2} f \right. \\
&\quad \left. + \frac{d-2}{2r} f' + \mu^2 \right). \quad (22)
\end{aligned}$$

Now, by applying the operator of Eq. (9) to Eq. (21) and using Eqs. (7)-(8) and the definition of  $u_{12}$  given in Eq. (18) to reduce the order of the derivatives, one obtains the decoupled quartic order equation for  $u_2$  as

$$\mathcal{D}_\ell^{s=1}(f^{-1}\mathcal{D}_\ell^{s=0}(ru_2)) = 2\mu^2 f f' u_2, \quad (23)$$

with  $\mathcal{D}_\ell^{s=1}$  being given by

$$\begin{aligned}
\mathcal{D}_\ell^{s=1} &= -\partial_t^2 + \partial_{r_*}^2 \\
&\quad - f \left( \frac{\ell(\ell+d-3)}{r^2} + \frac{(d-2)(d-4)}{4r^2} f \right. \\
&\quad \left. - \frac{d-4}{2r} f' + \mu^2 \right). \quad (24)
\end{aligned}$$

The operator  $\mathcal{D}_\ell^{s=1}$  of Eq. (24) is the  $d$ -dimensional generalization of the four-dimensional operator appearing in [19], and  $\mathcal{D}_\ell^{s=1} + \mu^2 f$  being the operator ruling the dynamics of the scalar sector of the Maxwell field in  $d$  dimensions. The decoupled equation Eq. (23) shows that the presence of a nonzero mass  $\mu$  makes the degrees of freedom of the function  $u_2$  physical. On the other hand, if one performs the massless limit  $\mu^2 = 0$ , Eq. (23) becomes

$$\mathcal{D}_\ell^{s=1}|_{\mu=0}(f^{-1}\mathcal{D}_\ell^{s=0}|_{\mu=0}(ru_2)) = 0, \quad (25)$$

where  $\mathcal{D}_\ell^{s=0}|_{\mu=0}$  is the operator of Eq. (22) with  $\mu = 0$  and  $\mathcal{D}_\ell^{s=1}|_{\mu=0}$  is the operator of Eq. (24) with  $\mu = 0$ . Thus, in this limit, the equations completely factorize. This was found for four dimensions in [19, 50]. One can interpret the factorization by Eq. (25) in the following way. The solution to  $\mathcal{D}_\ell^{s=0}(ru_2) = 0$  describes the pure-gauge degree of freedom of the Maxwell field, i.e.,  $u_{12} = 0$ , see Eq. (21). The physical degree of freedom is described by the function  $u_{12}$  and it obeys the Maxwell scalar-type equation  $\mathcal{D}_\ell^{s=1}u_{12} = 0$ , see again Eq. (21). When one puts  $\partial_t^2 = -\omega^2$  this latter equation yields Eqs. (18)-(20).

The vector-type sector, on the other hand, can be shown to be gauge invariant, meaning that vector-type modes are ruled by Eq. (16) after setting the mass  $\mu$  to zero, i.e.,  $\mu = 0$ , in the potential of Eq. (17). Thus, from Eqs. (16) and (17) we write

$$\partial_{r_*}^2 u_3 + (\omega^2 - V_{\text{vm}})u_3 = 0, \quad (26)$$

with the potential

$$\begin{aligned} V_{\text{vm}} = f & \left( \frac{(d-4)(d-2)}{4l^2} \right. \\ & + \frac{(2\ell+d-4)(2\ell+d-2)}{4r^2} \\ & \left. + \frac{d(d-4)}{4r_h^2} \left( 1 + \frac{r_h^2}{l^2} \right) \left( \frac{r_h}{r} \right)^{d-1} \right), \quad (27) \end{aligned}$$

where again the subscript m stands for Maxwell.

#### IV. ANALYTICAL PROPERTIES OF PROCA AND MAXWELL QUASINORMAL MODES

##### A. Asymptotic behavior of the solutions and boundary conditions

###### 1. Proca field perturbations

To obtain the QNM solutions in Schwarzschild-AdS, one needs to impose appropriate boundary conditions at the horizon and at spatial infinity.

At the horizon, we have  $f(r_h) = 0$ , and all the potentials vanish, meaning that one should have at first order  $u \sim e^{\pm i\omega r_*}$  near the horizon. The only classically allowed boundary condition is then that there are only ingoing waves, i.e.,  $u \sim e^{-i\omega r_*}$  which in terms of the coordinate  $r$  can be written as

$$u_k(r) = \alpha_k^{r=r_h} (r - r_h)^{-\frac{i\omega}{f'(r_h)}}, \quad r \rightarrow r_h, \quad (28)$$

where  $\alpha_k^{r=r_h}$  is a constant, with  $k \in \{1, 2, 3\}$ , and we have expanded  $f(r) = f'(r_h)(r - r_h) + \mathcal{O}((r - r_h)^2)$ .

The suitable boundary conditions at spatial infinity in pure AdS were determined in [40], see also [54]. To address this question, one must study how the Proca field behaves at spatial infinity. Since the

effect of the black hole can be neglected asymptotically, the behavior of the Proca field near spatial infinity is essentially the same as the one found for pure AdS. Namely, near  $r = +\infty$ , all Proca solutions behave as  $u_k = \alpha_k^{r=\infty} r^{-\frac{1}{2}(1+\sqrt{(d-3)^2+4\mu^2 l^2})} + \beta_k^{r=\infty} r^{-\frac{1}{2}(1-\sqrt{(d-3)^2+4\mu^2 l^2})}$  where  $\alpha_k^{r=\infty}$  and  $\beta_k^{r=\infty}$  are constants, with  $k \in \{1, 2, 3\}$ . Now we have to impose conditions on the functions  $u_k$  so that they behave well at infinity. For  $d = 4$  and  $0 < \mu^2 l^2 < \frac{3}{4}$  the functions  $u_k$  are square-integrable in the sense of  $\int \bar{u}_k u_k dr_*$  for one-parameter family of boundary conditions that includes the Dirichlet boundary condition, the latter meaning  $u_k(r \rightarrow \infty) = 0$  which implies  $\beta_k^{r=\infty} = 0$ . For  $d = 4$  and  $\frac{3}{4} \leq \mu^2 l^2 < \infty$  the functions  $u_k$  are square-integrable only if one imposes a Dirichlet boundary condition  $\beta_k^{r=\infty} = 0$ . For  $d > 4$ , the functions  $u_k$  are square-integrable also only for  $\beta_k^{r=\infty} = 0$ , which corresponds to the Dirichlet boundary condition, see [40] for these conditions. In any case, throughout this work, we assume Dirichlet boundary conditions at spatial infinity, i.e.,  $u_k(r \rightarrow \infty) = 0$ , and so  $\beta_k^{r=\infty} = 0$ . Thus,

$$u_k = \alpha_k^{r=\infty} r^{-\frac{1}{2}(1+\sqrt{(d-3)^2+4\mu^2 l^2})}, \quad r \rightarrow \infty, \quad (29)$$

gives the behavior of the function  $u_k$  at infinity.

###### 2. Maxwell field perturbations

The boundary condition at the horizon for Maxwell field perturbations is

$$u_i(r) = \alpha_i^{r=r_h} (r - r_h)^{-\frac{i\omega}{f'(r_h)}}, \quad r \rightarrow r_h, \quad (30)$$

where  $\alpha_i^{r=r_h}$  is a constant with  $i \in \{1, 2, 3\}$ . Note that Eq. (30) for Maxwell is analogous to Eq. (28) for Proca, the difference is in the running of the subscripts  $i$  and  $k$ .

On the other hand, the behavior of the Maxwell field near spatial infinity is different from Proca. Near  $r = +\infty$ , the Maxwell solutions behave accordingly with the dimension  $d$  [40, 54]. Regarding the scalar-type sector, for  $d = 4$  the behavior is  $u_{12} = \alpha_{12}^{r=\infty} r^{-1} + \beta_{12}^{r=\infty}$ , for  $d = 5$  the behavior is  $u_{12} = \alpha_{12}^{r=\infty} r^{-\frac{1}{2}} + \beta_{12}^{r=\infty} r^{-\frac{1}{2}} \ln r$ , for  $d \geq 6$  the behavior is  $u_{12} = \alpha_{12}^{r=\infty} r^{2-\frac{d}{2}} + \beta_{12}^{r=\infty} r^{\frac{d}{2}-3}$ . Regarding the vector-type sector, for  $d \geq 4$  the behavior is  $u_3 = \alpha_3^{r=\infty} r^{1-\frac{d}{2}} + \beta_3^{r=\infty} r^{\frac{d}{2}-2}$  where  $\alpha_i^{r=\infty}$  and  $\beta_i^{r=\infty}$  are constants, with  $i \in \{1, 2, 3\}$ . For  $d = 4, 5, 6$ , a whole one-parameter family of boundary conditions can be imposed. Nonetheless, we assume boundary conditions that allow us to connect with the Proca perturbations and so we set  $\beta_i = 0$ . For  $d = 4$ , to connect with the Proca perturbations, we impose the Dirichlet boundary condition, which corresponds to setting  $u_i(r \rightarrow \infty) = 0$  and so  $\beta_i^{r=\infty} = 0$ . For  $d = 5$  for the scalar-type Maxwell perturbations, we have  $u_{12}(r \rightarrow \infty) = 0$  even for  $\beta_i^{r=\infty} \neq 0$ . In this case, we impose the Dirichlet-Neumann condition, that is, the vanishing of the dominant logarithmic term,

thus  $\beta_i^{r=\infty} = 0$  in  $d = 5$  as well. For  $d = 6$ , again to connect with the Proca perturbations, we impose the Dirichlet boundary condition,  $u_i(r \rightarrow \infty) = 0$  and so  $\beta_i^{r=\infty} = 0$ . For  $d \geq 7$ , the Dirichlet boundary condition is the only one that guarantees well-defined dynamics for the Maxwell field [40]. Thus, after all this discussion, the Maxwell field  $u_i$  at infinity can be written as

$$u_{12} = \begin{cases} \frac{\alpha_{12}^{r=\infty}}{r}, & r \rightarrow \infty, & d = 4, \\ \frac{\alpha_{12}^{r=\infty}}{r^{\frac{d}{2}-2}}, & r \rightarrow \infty, & d \geq 5, \end{cases}$$

$$u_3 = \frac{\alpha_3^{r=\infty}}{r^{\frac{d}{2}-1}}, \quad r \rightarrow \infty, \quad d \geq 4, \quad (31)$$

where the  $\alpha_i^{r=\infty}$  are constants, with  $i \in \{12, 3\}$ .

## B. Linear stability of Schwarzschild-AdS

### 1. Method

We now prove that, for the boundary conditions used, all the decoupled Schrödinger-like equations of Section III, i.e., the monopole mode and vector-type modes of the Proca field, and the scalar and vector-type modes of the Maxwell field, must yield QNM frequencies  $\omega$  with negative imaginary part, which amounts to say that Schwarzschild-AdS is linearly stable against such perturbations. The approach we use for the proof is well-known and can be found in, e.g., [13, 18, 31, 33, 38]. We consider a general coupled system of Schrödinger-like equations with a Hermitian potential  $\mathbf{V}$  with solutions  $\mathbf{u}$ ,

$$\frac{d^2 \mathbf{u}}{dr_*^2} + (\omega^2 - \mathbf{V}) \mathbf{u} = 0. \quad (32)$$

Multiplying the system given in Eq. (32) by  $\mathbf{u}^\dagger$  and integrating in the region of interest, one has an energy balance like equation

$$\left( \mathbf{u}^\dagger \frac{d\mathbf{u}}{dr_*} \right) \Big|_{r_*=-\infty}^{r_*=r_*^{(\infty)}} + \omega^2 \int_{-\infty}^{r_*^{(\infty)}} |\mathbf{u}|^2 dr_*$$

$$= \int_{-\infty}^{r_*^{(\infty)}} \left( \left| \frac{d\mathbf{u}}{dr_*} \right|^2 + \mathbf{u}^\dagger \mathbf{V} \mathbf{u} \right) dr_*, \quad (33)$$

where the first term means the difference between the evaluation at spatial infinity and the evaluation at the horizon, in this order. We can conveniently introduce an arbitrary operator given by

$$\mathbf{D} = \mathbf{I} \frac{d}{dr_*} + \mathbf{S}(r_*), \quad (34)$$

where  $\mathbf{S}$  must be Hermitian. Also, we use the boundary conditions at the horizon, i.e., Eq. (28) for Proca and

Eq. (30) for Maxwell, which sets one of the boundary terms to  $\mathbf{u}^\dagger \frac{d\mathbf{u}}{dr_*} = -i\omega |\mathbf{u}(-\infty)|^2$ . With these two considerations, the energy balance like equation, Eq. (33), becomes

$$i\omega A + \omega^2 B = \int_{-\infty}^{r_*^{(\infty)}} \left( |\mathbf{D}\mathbf{u}|^2 + \mathbf{u}^\dagger \bar{\mathbf{V}} \mathbf{u} \right) dr_* + C, \quad (35)$$

where

$$\bar{\mathbf{V}} = \mathbf{V} + \frac{d\mathbf{S}}{dr_*} - \mathbf{S}^2$$

$$A = |\mathbf{u}(-\infty)|^2, \quad B = \int_{-\infty}^{r_*^{(\infty)}} |\mathbf{u}|^2 dr_*, \quad (36)$$

$$C = - \left( \mathbf{u}^\dagger \frac{d\mathbf{u}}{dr_*} \right) \Big|_{r_*=r_*^{(\infty)}} - \left( \mathbf{u}^\dagger \mathbf{S} \mathbf{u} \right) \Big|_{r_*=-\infty}^{r_*=r_*^{(\infty)}}.$$

In order to proceed, we must require that the effective potential  $\bar{\mathbf{V}}$  must be positive definite and that  $C$  must be a real positive number. The main reason for the introduction of  $\mathbf{S}$  is related to the cases where  $\mathbf{V}$  is not positive definite, as one can choose an  $\mathbf{S}$  so that a modified potential  $\bar{\mathbf{V}}$  is positive definite. This procedure is called the  $S$ -deformation technique. The requirement of  $C$  being a real positive number can be achieved by the combination of the boundary condition at spatial infinity and the choice of  $\mathbf{S}$ . One now can obtain the imaginary part of Eq. (35) as

$$\Re(\omega)A + 2\Re(\omega)\Im(\omega)B = 0. \quad (37)$$

Since  $A$  and  $B$  are positive and nonzero, one has that  $\Im(\omega) < 0$  if  $\Re(\omega) \neq 0$ . In the case  $\Re(\omega) = 0$ , one can consider the real part of Eq. (35), written as

$$-\Im(\omega)A - \Im(\omega)^2 B$$

$$= \int_{-\infty}^{r_*^{(\infty)}} \left( |\mathbf{D}\mathbf{u}|^2 + \mathbf{u}^\dagger \bar{\mathbf{V}} \mathbf{u} \right) dr_* + C. \quad (38)$$

Since the right-hand side is positive with the considerations above, with  $A$  and  $B$  also positive, then  $\Im(\omega) < 0$ .

Therefore, the method used here guarantees that if  $\mathbf{V}$  is Hermitian, if one can pick an  $\mathbf{S}$  such that  $\mathbf{V}$  is positive definite, and if the choice of  $\mathbf{S}$  and the boundary condition at spatial infinity lead to a real positive  $C$ , then the QNM frequencies have a negative imaginary part, yielding thus linear stability. Let us apply this technique to Proca and Maxwell field perturbations.

### 2. Proca field perturbations

For scalar-type Proca field perturbations, this technique can only be addressed for the monopole mode,  $\ell = 0$ , with the potential given by  $V_{s11}$  in Eq. (15). In this case, although the monopole potential is negative in a region near the horizon, one can consider

the effective potential  $\bar{V} = V + \frac{dS}{dr_*} - S^2 = f\mu^2$ , see Eq. (36), with  $S = \frac{(d-2)f}{2r}$ . One has that  $\bar{V} \geq 0$ ,  $S(r = r_h) = 0$ ,  $S|u|^2|_{r \rightarrow +\infty} \sim \lim_{r \rightarrow +\infty} r^{-\sqrt{(d-3)^2 + 4\mu^2 l^2}} = 0$ , and also  $C = 0$  due to the Dirichlet boundary condition, so that the results from Eqs. (37) and (38) can be used. Schwarzschild-AdS is then linearly stable against monopole Proca field perturbations. Higher multipoles of scalar-type Proca field perturbations are governed by the coupled potential Eqs. (14) and (15), which is non-Hermitian. This leads to additional terms in Eqs. (37) and (38), making it impossible to draw any conclusions about stability through this technique. One might argue that there could be an  $\mathcal{S}$  function transforming the non-Hermitian potential into a Hermitian one. However, this is not the case, as for the S-deformation technique to be useful, one also needs to ensure that  $\mathcal{S}$  itself is Hermitian. From the relation between the old potential and the transformed one, see Eq. (36), if  $\bar{\mathcal{V}} \equiv \mathcal{V} + \frac{d\mathcal{S}}{dr_*} - \mathcal{S}^2$  is Hermitian,  $\mathcal{V}$  needs to be Hermitian. Thus, in this case, one can only test stability by computing numerically the QNM spectrum.

For vector-type Proca field perturbations, the potential  $V_v$  ruling them given in Eq. (17), is positive in the region of interest. One can therefore choose  $S = 0$  and due to the Dirichlet boundary condition,  $C$  also vanishes. It follows then from Eqs. (37) and (38) that Schwarzschild-AdS is linearly stable against such perturbations.

### 3. Maxwell field perturbations

For the scalar-type Maxwell perturbations, the potential is given by Eq. (20). One must split the analysis into the different dimensions. For  $d = 4$ , the potential is positive and Hermitian, the Dirichlet condition leads to a vanishing  $C$ , and so one has  $S = 0$ . So there is linear stability. Note that in  $d = 4$ , the scalar-type Maxwell potential is equal to the vector-type Maxwell potential, For  $d = 5$ , the potential is unbounded from below, such that  $V \rightarrow -\infty$  as  $r \rightarrow \infty$ . One can choose an  $S$  as  $S = \frac{f}{2r}$  so that  $\bar{V}$  becomes positive. Moreover, by using the Dirichlet-Neumann condition, which we are using in  $d = 5$ , and using the chosen  $S$ , surprisingly, the term  $C$  vanishes. Therefore, we have the necessary requisites to apply Eqs. (37) and (38). So there is linear stability. For  $d \geq 6$ , the potential dips to negative values near the horizon. One must then choose  $S = \frac{(d-4)f}{2r}$  to have  $\bar{V} \geq 0$ . By using the chosen  $S$  and the Dirichlet boundary condition, the term  $C$  vanishes, and so from Eqs. (37) and (38) there is linear stability.

For vector-type Maxwell perturbations, the potential is given by Eq. (27). It is positive and Hermitian and also the Dirichlet boundary condition ensures a vanishing  $C$ , and so from Eq. (37) and (38) with  $S = 0$ , there is linear stability.

## C. Isospectrality between scalar-type and vector-type perturbations in large black holes

### 1. Initial considerations

Proca fields in  $d = 4$  do not show isospectrality between scalar-type and vector-type perturbations. On the other hand, it is well-known that scalar-type and vector-type Maxwell field perturbations are exactly isospectral in  $d = 4$  [33]. Here we investigate isospectrality in  $d$  dimensions and show in what conditions it might occur.

### 2. Proca field perturbations and isospectrality

For Proca, looking at the scalar potential matrix  $V_s$  with components in Eqs. (15) and the vector potential  $V_v$  in Eq. (17), respectively, it is clear they are completely different, even in  $d = 4$ . This may indicate that isospectrality between the two types of perturbation for a Proca field can never be realized. Indeed, this is supported by numerical calculations in the Sec. VI and in [50] for  $d = 4$ .

### 3. Maxwell field perturbations and isospectrality

For Maxwell, we look at the scalar potential  $V_{sm}$  and the vector potential  $V_{vm}$  in Eqs. (20) and (27), respectively. If we restrict their expressions to  $d = 4$  it becomes clear that the potentials are equal and so the scalar and vector perturbations are isospectral. On the other hand, from Eqs. (20) and (27) it is immediate that  $V_{sm}$  and  $V_{vm}$  are different and it may implicate that isospectrality breaks for higher dimensions,  $d \geq 5$ . This is in fact supported by the numerical results in the Sec. VI.

It turns out that for the Maxwell field, as one analyzes large black holes with  $\frac{r_h}{l} \gg \ell$ , the scalar-type and vector-type Maxwell perturbations tend to be isospectral in higher dimensions, although nothing in the potentials suggests such behavior. Indeed, Maxwell scalar-type perturbations are governed by the potential given in Eq. (20), which for large black holes in  $d \geq 5$  reduces to

$$V_{sm}^{\frac{r_h}{l} \gg \ell} = f \left( \frac{(d-4)(d-6)}{4l^2} - \frac{(3d-8)(d-4)}{4l^2} \left( \frac{r_h}{r} \right)^{d-1} \right). \quad (39)$$

Maxwell vector-type perturbations are governed by the potential of Eq. (27), which for large black holes in  $d \geq 5$  can be written as

$$V_{vm}^{\frac{r_h}{l} \gg \ell} = f \left( \frac{(d-2)(d-4)}{4l^2} + \frac{d(d-4)}{4l^2} \left( \frac{r_h}{r} \right)^{d-1} \right). \quad (40)$$

The potentials of Eqs. (39) and (40) can be written as

$$\begin{aligned} V_{\text{sm}}^{\frac{r_h}{l} \gg \ell} &= W^2 + \frac{dW}{dr_*}, \\ V_{\text{vm}}^{\frac{r_h}{l} \gg \ell} &= W^2 - \frac{dW}{dr_*}, \\ W(r) &\equiv -\frac{(d-4)}{2l^2} \left( 1 - \left( \frac{r_h}{r} \right)^{d-1} \right) r. \end{aligned} \quad (41)$$

Following a procedure developed by Chandrasekhar [7], see also [33], one can check that Eqs. (19) and (26) can be written as

$$\begin{aligned} u_{12} &= \frac{1}{\sqrt{\beta - \omega^2}} \left( W u_3 + \frac{d u_3}{d r_*} \right), \\ u_3 &= \frac{1}{\sqrt{\beta - \omega^2}} \left( -W u_{12} + \frac{d u_{12}}{d r_*} \right), \end{aligned} \quad (42)$$

respectively. Supposing that  $\omega$  is a QNM of  $u_3$ , one must have  $u_3 = \alpha_3^{r=r_h} e^{-i\omega r_*}$  when  $r \rightarrow r_h$  and  $u_3 = 0$  when  $r \rightarrow \infty$ . The behavior of  $u_{12}$  near the horizon and near spatial infinity then yields, from Eq. (42),  $u_{12} = -\alpha_3^{r=r_h} e^{-i\omega r_*}$  when  $r \rightarrow r_h$  and  $u_{12} = \frac{1}{\sqrt{-\omega^2}} (W u_3 + f \frac{d u_3}{d r})|_{r=\infty}$  when  $r \rightarrow \infty$ . The behavior of  $u_3$  near spatial infinity is given by Eq. (31), so that  $(W u_3 + f \frac{d u_3}{d r})|_{r=\infty} \sim \frac{d-3}{l^2} r^{2-\frac{d}{2}}|_{r=\infty}$ , which vanishes for  $d \geq 5$ , i.e.,  $u_{12} \rightarrow 0$ . Thus, if  $\omega$  is a QNM frequency of  $u_3$ , it is also a QNM frequency of  $u_{12}$  when  $r \rightarrow \infty$ , and so the scalar-type and vector-type modes tend to isospectrality when  $\frac{r_h}{l} \gg \ell$ . Note that we do not consider modes that have  $\omega^2 = 0$ , as it is not expected that they exist.

## D. Low purely damped modes for large black holes

### 1. Initial considerations

Scalar-type and vector-type gravitational perturbations in large Schwarzschild-AdS black holes possess low frequency modes, which play a role in the AdS/CFT correspondence, as they describe the behavior of the dual field theory in the hydrodynamic regime. These gravitational modes were found numerically [33, 36] and analytically [41] in  $d = 4$ , and were found numerically [43] in  $d = 5$ . Using a perturbative approach, in [44] it was found the analytical expression for these modes in  $d$  dimensions, whose results agree not only with the previous numerical results, but also with previous analytical results from the dual field theory side.

In this section, we employ the perturbative method of [44] to study if such low-frequency modes exist in Proca and Maxwell fields. We mention in passing Proca field modes and argue that for scalar-type Proca perturbations the approach does not seem to be feasible, as this would require solving a coupled system, while the results may follow for the vector-type Proca perturbations from the vector-type Maxwell case, indeed, in  $d \geq 4$ , vector-type

Proca perturbations do not possess such low-frequency modes. We perform an exhaustive analysis for Maxwell field perturbations. For scalar-type Maxwell perturbations we show that in  $d = 4$  there are no such modes. In  $d \geq 5$  we show that scalar-type Maxwell perturbations in large Schwarzschild-AdS black holes have purely damped modes that scale with the inverse of the radius of the black hole. In  $d \geq 4$ , vector-type Maxwell perturbations do not possess low-frequency modes.

We must note that in [33, 50], for  $d = 4$ , both the Proca and Maxwell fields have a finite number of almost purely damped high modes for large black holes, both in the scalar and the vector sector. However, these modes scale with the event horizon radius and so they must not be confused with the low purely damped modes that we are analyzing here.

### 2. Proca field perturbations

For Proca scalar field perturbations and modes we will not pursue an analytical study as this would require solving perturbatively the coupled system of Eq. (13). The existence of such modes will be considered numerically.

For vector field perturbations and modes, we will analyze the corresponding modes in the Maxwell theory and show that the analysis can be extended to the vector-type Proca perturbations by taking into account the mass  $\mu$  of the field.

### 3. Maxwell field perturbations

We now do first scalar-type perturbations for the Maxwell field. To check for the existence of the low pure damped modes, we must analyze the solution in the limit of very large black holes, i.e.,  $r_h \rightarrow \infty$ , while keeping  $\hat{l}^2$ ,  $\hat{\ell}$ , and  $\hat{\omega}$  small but fixed, these being defined through

$$\hat{l}^2 = \frac{l^2}{r_h^2}, \quad \hat{\ell}^2 = \hat{l}^2 \ell (\ell + d - 3), \quad \hat{\omega} = \hat{l}^2 \omega r_h. \quad (43)$$

Following [44], we use a transformation from the variable  $r$  to  $\zeta$  and from the function  $u_{12}$  to  $U_{12}$  by

$$\zeta = \left( \frac{r_h}{r} \right)^{d-3}, \quad u_{12}(\zeta) = (1 - \zeta)^{\frac{i\hat{\omega}}{(d-1)+(d-3)\hat{l}^2}} U_{12}(\zeta). \quad (44)$$

Then, with these new definitions and variables Eq. (19) turns into

$$A_{\hat{l}^2} \partial_\zeta^2 U_{12} + B_{\hat{l}^2, \hat{\omega}} \partial_\zeta U_{12} + C_{\hat{l}^2, \hat{\omega}, \hat{\ell}^2} U_{12} = 0, \quad (45)$$

with coefficients

$$\begin{aligned}
A_{\hat{l}^2} &= (d-3)^2 \left( \zeta^3 - \zeta^{\frac{2d-8}{d-3}} \right) + (d-3)^2 (\zeta-1) \zeta^2 \hat{l}^2, \\
B_{\hat{l}^2, \hat{\omega}} &= (d-3) \left( (2d-5) \zeta^2 - (d-4) \zeta^{\frac{d-5}{d-3}} \right) \\
&\quad + (d-3) \left( (2d-5) \zeta^2 + (2-d) \zeta \right) \hat{l}^2 \\
&\quad + \frac{2i(d-3)^2 \left( \zeta^{\frac{2d-8}{d-3}} - \zeta^3 \right)}{(d-1)(\zeta-1)} \hat{\omega} + \mathcal{O}(\varepsilon^2), \\
C_{\hat{l}^2, \hat{\omega}, \hat{\ell}^2} &= \frac{(d-4)}{4} \left( (d-6) \zeta^{-\frac{2}{d-3}} + (8-3d) \zeta \right) \\
&\quad + \frac{1}{4} (d-4) \left( (d-2) + (8-3d) \zeta \right) \hat{l}^2 \\
&\quad - \frac{i(d-3) \zeta}{(d-1)(\zeta-1)^2} \left( (d+u-4) \zeta^{-\frac{2}{d-3}} \right. \\
&\quad \left. + \zeta(d(u-2) - 2\zeta + 5) \right) \hat{\omega} + \hat{\ell}^2 + \mathcal{O}(\varepsilon^2),
\end{aligned} \tag{46}$$

where an expansion up to first order was done in  $\hat{l}^2$ ,  $\hat{\ell}^2$ , and  $\hat{\omega}$ , and the parameter  $\varepsilon$  can be understood as the smallness of these three parameters, meaning  $\hat{l}^2 \sim \varepsilon$ ,  $\hat{\ell}^2 \sim \varepsilon$ , and  $\hat{\omega} \sim \varepsilon$ . The idea now is to consider a perturbative expansion of the solution for  $U_{12}$  as

$$U_{12} = U_{12}^{(0)} + U_{12}^{(1)} + \mathcal{O}(\varepsilon^2), \tag{47}$$

with  $\varepsilon \ll 1$ , where  $\mathcal{O}(U_{12}^{(0)}) = \mathcal{O}(1)$  and  $\mathcal{O}(U_{12}^{(1)}) = \mathcal{O}(\varepsilon)$ . At zeroth order, we obtain

$$\mathcal{H}_0 U_{12}^{(0)} = 0, \quad \mathcal{H}_0 \equiv A_0 \partial_\zeta^2 + B_{0,0} \partial_\zeta + C_{0,0,0}, \tag{48}$$

with  $A_0 = A_{\hat{l}^2=0}$ ,  $B_{0,0} = B_{\hat{l}^2=0, \hat{\omega}=0}$ ,  $C_{0,0,0} = C_{\hat{l}^2=0, \hat{\omega}=0, \hat{\ell}^2=0}$ . The solutions to Eq. (48) are written as

$$U_{12}^{(0)}(\zeta) = \tilde{\gamma}_{12}^{(0)} \tilde{U}_{12}^{(0)}(\zeta) + \hat{\gamma}_{12}^{(0)} \hat{U}_{12}^{(0)}(\zeta), \tag{49}$$

with  $\tilde{\gamma}_{12}^{(0)}$  and  $\hat{\gamma}_{12}^{(0)}$  constants, and

$$\tilde{U}_{12}^{(0)}(\zeta) = \zeta^{\frac{d-4}{2(d-3)}}, \quad \hat{U}_{12}^{(0)}(\zeta) = \zeta^{\frac{d-4}{2(d-3)}} \int^\zeta d\zeta' \frac{\mathcal{W}(\zeta')}{\zeta'^{\frac{d-4}{d-3}}}, \tag{50}$$

where  $\mathcal{W}(\zeta)$  is the Wronskian with the following dependence  $\mathcal{W}(\zeta) \sim \zeta^{-\frac{d-4}{d-3}} \left( 1 - \zeta^{\frac{d-1}{d-3}} \right)^{-1}$ . The boundary condition at the horizon, described in these coordinates as  $\zeta = 1$ , imposes  $\hat{\gamma}_{12}^{(0)} = 0$  in Eq. (49) for all spacetime dimensions, since  $\hat{U}_{12}^{(0)} \sim \ln(1-\zeta)$ . For  $d = 4$ , the Dirichlet boundary condition is only satisfied if  $\tilde{\gamma}_{12}^{(0)} = 0$ , which yields the trivial solution  $U_{12}^{(0)} = 0$ . This implies the absence of the low pure damped modes for the case of  $d = 4$ . The Dirichlet-Neumann boundary condition for  $d = 5$  and the Dirichlet boundary condition for  $d > 5$  at spatial infinity, described by  $\zeta = 0$ , are automatically

satisfied. Carrying on for the case of  $d \geq 5$ , at first order Eqs. (45)-(47) yield

$$\mathcal{H}_0 U_{12}^{(1)} = -\mathcal{H}_1 U_{12}^{(0)}, \tag{51}$$

where  $\mathcal{H}_1 = A_{\hat{l}^2} \partial_\zeta^2 + B_{\hat{l}^2, \hat{\omega}} \partial_\zeta + C_{\hat{l}^2, \hat{\omega}, \hat{\ell}^2} - \mathcal{H}_0$ . It can be shown that  $\left( A_{\hat{l}^2} \partial_\zeta^2 + B_{\hat{l}^2, 0} \partial_\zeta + C_{\hat{l}^2, 0, 0} \right) \tilde{U}_{12}^{(0)} = 0$ , so that if one neglects the  $\hat{l}^2$  terms in the forthcoming calculations, the results still remain valid at  $\mathcal{O}(\hat{l}^2)$ . The particular solutions to Eq. (51) can be written as

$$\begin{aligned}
U_{12}^{(1)}(\zeta) &= \hat{U}_{12}^{(0)}(\zeta) \int_1^\zeta d\zeta' \frac{\tilde{U}_{12}^{(0)} \mathcal{H}_1 U_{12}^{(0)}}{A_0 \mathcal{W}} \\
&\quad + \tilde{U}_{12}^{(0)}(\zeta) \int_1^\zeta d\zeta' \frac{\hat{U}_{12}^{(0)} \mathcal{H}_1 U_{12}^{(0)}}{A_0 \mathcal{W}},
\end{aligned} \tag{52}$$

where the lower limit in the integrals was chosen to be  $\zeta' = 1$  so that the boundary condition at the horizon is automatically satisfied. The possible divergent term at spatial infinity is the first line in Eq. (52), i.e., the term proportional to  $\hat{U}_{12}^{(0)}$ . Imposing the boundary condition at spatial infinity, one must require that  $\int_1^0 d\zeta' \frac{\tilde{U}_{12}^{(0)} \mathcal{H}_1 U_{12}^{(0)}}{A_0 \mathcal{W}} = 0$ . This last condition, together with  $U_{12}^{(0)} \sim \zeta^{\frac{d-4}{2(d-3)}}$ , see Eq. (50), gives precisely the equation for the low pure damped QNM frequencies

$$\omega = -i \frac{\ell(\ell + d - 3)}{(d-3)r_h}. \tag{53}$$

Note again that these modes do not exist for  $d = 4$ , since Eq. (45) has no nontrivial solutions satisfying the appropriate boundary conditions. The modes of Eq. (53) only exist for  $d \geq 5$ .

We continue with the analysis now for vector-type perturbations of the Maxwell field. For vector-type Maxwell field perturbations, we can perform the same transformations as in the scalar-type perturbations, which now are

$$\zeta = \left( \frac{r_h}{r} \right)^{d-3}, \quad u_3(\zeta) = (1-\zeta)^{\frac{i\hat{\omega}}{(d-1)+(d-3)\hat{\ell}^2}} U_3(\zeta), \tag{54}$$

see Eq. (44). Doing the same procedure that was done for scalar-type perturbations, the vector-type solutions at zeroth order of  $\hat{\ell}^2 \sim \varepsilon$ ,  $\hat{\omega} \sim \varepsilon$  and  $\hat{l}^2 \sim \varepsilon$  are

$$U_3^{(0)}(\zeta) = \tilde{\gamma}_3^{(0)} \tilde{U}_3^{(0)}(\zeta) + \hat{\gamma}_3^{(0)} \hat{U}_3^{(0)}(\zeta), \tag{55}$$

where  $\tilde{\gamma}_3^{(0)}$  and  $\hat{\gamma}_3^{(0)}$  are constants, with

$$\tilde{U}_3^{(0)}(\zeta) = \zeta^{-\frac{d-4}{2(d-3)}}, \quad \hat{U}_3^{(0)}(\zeta) = \zeta^{-\frac{d-4}{2(d-3)}} \int^\zeta d\zeta' \zeta'^{\frac{d-4}{d-3}} \mathcal{W}(\zeta'), \tag{56}$$

and the Wronskian being  $\mathcal{W} \sim \zeta^{-\frac{d-4}{d-3}} \left( 1 - \zeta^{\frac{d-1}{d-3}} \right)^{-1}$ . Since  $\tilde{U}_3^{(0)}$  does not satisfy the Dirichlet boundary condition at  $\zeta = 0$  for any spacetime dimension, one needs

to impose  $\hat{\gamma}_3^{(0)} = 0$  in Eq. (55). As before, the boundary condition at the horizon, described in these coordinates as  $\zeta = 1$ , imposes  $\hat{\gamma}_2^{(0)} = 0$  in Eq. (55) for all space-time dimensions, since  $\hat{U}_3^{(0)} \sim \ln(1 - \zeta)$ . Thus, there are no nontrivial perturbative solutions, and vector-type Maxwell perturbations do not exhibit low pure damped modes. Such conclusions may be extended to the vector-type Proca perturbations by considering  $\hat{\mu}^2 = \hat{l}^2 \mu^2 r_h^2$  as a perturbation, with  $\mathcal{O}(\hat{\mu}^2) = \mathcal{O}(\varepsilon)$ .

#### 4. Comments

A comment is in order regarding the results from the two last sections. In Sec. IVC, it was proved that, for large black holes, Maxwell scalar-type and vector-type modes tend to isospectrality. On the other hand, the study from Sec. IVD reveals that there are low frequency modes for scalar-type perturbations that do not exist for vector-type perturbations. There is an apparent contradiction between the two results, but this is only due to the degree of the approximation in both results. Note, that Eq. (41) only holds when one neglects the angular momentum number  $\ell$  and one considers the large black hole approximation, i.e.,  $f(r) \sim \frac{r^2}{l^2} - \frac{r_h^2}{l^2} (\frac{r_h}{r})^{d-3}$ . If  $\ell$  is restored and the full expression for  $f(r)$  is considered, then there is no  $W$  that satisfies Eq. (41), and isospectrality cannot be established. Furthermore, the low pure damped modes scale with the inverse of the event horizon radius and so it is expected that for infinite large black holes these modes tend to a zero frequency. In turn, note from Eq. (53), that if one neglects the angular momentum number  $\ell$ , there are no low frequency scalar-type modes. Thus, the results from Sec. IVC and Sec. IVD are consistent. In fact, we checked numerically that such low frequency modes do not exist for the Schrödinger-like equation with potential Eq. (39) and  $f(r) \sim \frac{r^2}{l^2} - \frac{r_h^2}{l^2} (\frac{r_h}{r})^{d-3}$ , see below Section VI.

### V. NUMERICAL INTEGRATION METHODS FOR THE COMPUTATION OF THE QUASINORMAL MODE FREQUENCIES OF PROCA AND MAXWELL FIELDS IN SCHWARZSCHILD-ADS

#### A. Numerical integration methods for the Proca field: Decoupled and coupled Schrödinger-like equations

##### 1. The shooting method

(a) *Scalar-type  $\ell = 0$  monopole Proca field and vector-type Proca field: Decoupled Schrödinger-like equation*

The numerical integration method to obtain the QNMs for the Proca field in  $d$ -dimensions can be based on integrating the Schrödinger-like equation using the shooting

method [6, 18, 19, 21, 45]. One starts from a point near the horizon, with radius  $r_i = r_h(1 + \epsilon)$ ,  $\epsilon \ll 1$ , where it is imposed the boundary condition at the horizon, Eq. (28). The method works for Proca monopole modes, Proca vector-type perturbation modes, and Maxwell modes. We explain now in detail the method applied for Proca vector-type perturbation modes which is the more involved case, the other cases follow with ease.

The expansion of the Proca function  $u_3$  evaluated at  $r_i$  is given by

$$\begin{aligned} u_3(r_i) &= (r_i - r_h)^{-\frac{i\omega}{f'(r_h)}} \sum_{j=0}^{N_i} a_{(3)j} (r_i - r_h)^j, \\ \partial_r u_3(r_i) &= (r_i - r_h)^{-\frac{i\omega}{f'(r_h)} - 1} \\ &\times \sum_{j=0}^{N_i} \left( j a_{(3)j} - \frac{i\omega}{f'(r_h)} a_{(3)j} \right) (r_i - r_h)^j, \end{aligned} \quad (57)$$

where  $N_i$  is the order at which the expansion is truncated, and  $a_{(3)j}$  are coefficients of the expansion in  $r$  near the horizon. The coefficients  $a_{(3)j}$  are found by substituting  $u_3(r) = (r - r_h)^{-\frac{i\omega}{f'(r_h)}} \sum_{j=0}^{N_i} a_{(3)j} (r - r_h)^j$  in Eq. (16) and equating the coefficients corresponding to each power term  $(r - r_h)$ , in the first  $N_i$  expansion terms. This expansion of the Proca function  $u_3$  evaluated at  $r_i$  as given in Eq. (57) is taken as the initial condition for the initial value problem. At a large radius  $r_f = \kappa r_h$ , with  $\kappa \gg 1$ , one also expands the field using the asymptotic behavior that obeys the boundary conditions that we impose, in this case the Dirichlet boundary condition. The expansion of the function  $u_3$ , now evaluated at  $r_f$ , is given by

$$\begin{aligned} u_3(r_f) &= u_3^{r \rightarrow \infty}(r_f) \sum_{j=0}^{N_f} b_{(3)j} r_f^{-j}, \\ \partial_r u_3(r_f) &= \frac{\partial_r u_3^{r \rightarrow \infty}(r_f)}{u_3^{r \rightarrow \infty}(r_f)} u_3(r_f) \\ &- u_3^{r \rightarrow \infty}(r_f) \sum_{j=0}^{N_f} j b_{(3)j} r_f^{-j-1}, \end{aligned} \quad (58)$$

where  $u_3^{r \rightarrow \infty}(r) = r^{-\frac{1}{2} - \frac{1}{2}\sqrt{(d-3)^2 + 4\mu^2 l^2}}$  and  $b_{(3)j}$  are the expansion coefficients at very large radius. Again, the coefficients  $b_{(3)j}$  can be determined in terms of  $b_{(3)0}$  by inserting the series  $u_3(r) = u_3^{r \rightarrow \infty}(r) \sum_{j=0}^{N_f} b_{(3)j} r^{-j}$  into Eq. (16) and equating the coefficients corresponding to each power term  $\frac{1}{r}$ , in the first  $N_f$  expansion terms. This expansion of the Proca function  $u_3$  evaluated at  $r_f$  as given in Eq. (58) is taken as the initial condition for a distinct initial value problem.

One now chooses, without loss of generality,  $a_{(3)0} = 1$  and  $b_{(3)0} = 1$ . The method now consists in performing two integrations, through numerical methods, of Eq. (16). One integration is carried from  $r = r_i$  up to the middle point  $r = r_m$ , i.e.,  $r_i < r_m < r_f$ , using the

initial values of Eq. (57). In turn, the other integration is carried from  $r = r_f$  down to  $r = r_m$ , using the initial values of Eq. (58). Since the two solutions, say  $u_{3r_i}(r)$  and  $u_{3r_f}(r)$ , must be linearly dependent at  $r = r_m$ , the problem amounts to finding the root of the Wronskian

$$\mathcal{W}(u_{3r_i}, u_{3r_f}; r_m) = (u_{3r_i} u'_{3r_f} - u_{3r_f} u'_{3r_i})|_{r=r_m} = 0, \quad (59)$$

which must be satisfied for the QNM frequency  $\omega$ . We note that the Wronskian is independent of  $r$ , so that the choice of  $r = r_m$  does not affect the results.

We can apply this method for the monopole scalar-type Proca field  $u_1$  with  $u_2 = 0$  and with potential  $V_{s11}$  in Eq. (15), for the vector-type Proca field  $u_3$  as just explained, for the scalar-type Maxwell field  $u_{12}$  with potential given in Eq. (20), and for the vector-type Maxwell field  $u_3$  in Eq. (27). The expansions near the horizon are similar, while for the expansions in the far radius  $r_f$ , one must use the asymptotic behavior obeying the boundary conditions for each field.

(b) *Scalar-type  $\ell \geq 1$  Proca field: Coupled equations*

For the coupled modes, i.e.,  $\ell \geq 1$  scalar-type Proca field modes in  $d$ -dimensions, one must extend the shooting method procedure dimensions according to [19, 21]. We perform the expansion of the functions  $u_1$  and  $u_2$  near the horizon at  $r_i = r_h(1 + \epsilon)$ , with  $\epsilon \ll 1$ , as

$$\begin{aligned} u_k(r_i) &= (r_i - r_h)^{-\frac{i\omega}{f'(r_h)}} \sum_{j=0}^{N_i} a_{(k)j} (r_i - r_h)^j, \\ \partial_r u_k(r_i) &= (r_i - r_h)^{-\frac{i\omega}{f'(r_h)} - 1} \\ &\times \sum_{j=0}^{N_i} \left( j a_{(k)j} - \frac{i\omega}{f'(r_h)} a_{(k)j} \right) (r_i - r_h)^j, \end{aligned} \quad (60)$$

for  $k = \{1, 2\}$  in this case, with  $N_i$  being the truncation order, where  $a_{(k)j}$  are the expansion coefficients near the horizon. By putting the expansion in the system of coupled equations Eq. (13), one determines the coefficients of the expansion  $a_{(k')j}$  in function of  $a_{(k)0}$ . One also performs the expansion of the functions  $u_1$  and  $u_2$  at a large radius  $r_f = \kappa r_h$ , where  $\kappa \gg 1$ , as

$$\begin{aligned} u_k(r_f) &= u_k^{r \rightarrow \infty}(r_f) \sum_{j=0}^{N_f} b_{(k)j} r_f^{-j}, \\ \partial_r u_k(r_f) &= \frac{\partial_r u_k^{r \rightarrow \infty}(r_f)}{u_k^{r \rightarrow \infty}(r_f)} u_k(r_f) \\ &- u_k^{r \rightarrow \infty}(r_f) \sum_{j=0}^{N_f} j b_{(k)j} r_f^{-j-1}, \end{aligned} \quad (61)$$

where  $u_k^{r \rightarrow \infty}(r) = r^{-\frac{1}{2} - \frac{1}{2}\sqrt{(d-3)^2 + 4\mu^2 l^2}}$  and  $b_{(k)j}$  are the expansion coefficients at very large radius. One then uses Eq. (13) to determine the  $b_{(k')j}$  in function of  $b_{(k)0}$ , by considering the first  $N_f$  terms of the expansion in  $\frac{1}{r}$ .

The expansions in Eqs. (60) and (61) are treated as initial values for the integration of the coupled system in Eq. (13), as in the decoupled case. Since the coupled system in Eq. (13) is linear, the integration with initial values given in Eq. (60) yields a linear combination of independent functions with coefficients  $a_{(k)0}$ . We thus perform two integrations, from  $r_i$  to  $r_m$ , for the pairs  $(a_{(1)0}, a_{(2)0}) = (1, 0)$  and  $(a_{(1)0}, a_{(2)0}) = (0, 1)$ , yielding the functions  $(u_{1r_i})_{a_{(1)0}}$  and  $(u_{2r_i})_{a_{(1)0}}$  for the first pair, and  $(u_{1r_i})_{a_{(2)0}}$  and  $(u_{2r_i})_{a_{(2)0}}$  for the second pair. Similarly, the integration of Eq. (13) with initial conditions Eq. (61) gives a linear combination of independent functions with coefficients  $b_{(k)0}$ , and we perform two integrations, from  $r_f$  to  $r_m$ , for the pairs  $(b_{(1)0}, b_{(2)0}) = (1, 0)$  and  $(b_{(1)0}, b_{(2)0}) = (0, 1)$ , with solutions  $(u_{1r_f})_{b_{(1)0}}$  and  $(u_{2r_f})_{b_{(1)0}}$  for the first pair, and  $(u_{1r_f})_{b_{(2)0}}$  and  $(u_{2r_f})_{b_{(2)0}}$  for the second pair. Linear dependence of  $u_1$  and  $u_2$  can be encapsulated in the vanishing of the Wronskian of the system at  $r_m$

$$\begin{aligned} \mathcal{W}(\mathbf{u}_{r_i}, \mathbf{u}_{r_f}; r_m) &= \\ \det \begin{pmatrix} (u_{1r_i})_{a_{(1)0}} & (u_{1r_i})_{a_{(2)0}} & (u_{1r_f})_{b_{(1)0}} & (u_{1r_f})_{b_{(2)0}} \\ (u_{2r_i})_{a_{(1)0}} & (u_{2r_i})_{a_{(2)0}} & (u_{2r_f})_{b_{(1)0}} & (u_{2r_f})_{b_{(2)0}} \\ (u'_{1r_i})_{a_{(1)0}} & (u'_{1r_i})_{a_{(2)0}} & (u'_{1r_f})_{b_{(1)0}} & (u'_{1r_f})_{b_{(2)0}} \\ (u'_{2r_i})_{a_{(1)0}} & (u'_{2r_i})_{a_{(2)0}} & (u'_{2r_f})_{b_{(1)0}} & (u'_{2r_f})_{b_{(2)0}} \end{pmatrix} \\ &= 0, \end{aligned} \quad (62)$$

where  $\mathbf{u}_{r_i}$  and  $\mathbf{u}_{r_f}$  are the vectors of functions resulting from the integration of the coupled system with initial values at  $r_i$  and  $r_f$ , respectively, and the determinant is evaluated at  $r = r_m$ . The vanishing of the Wronskian in Eq. (62) yields the QNM frequencies of the scalar-type Proca field. We note that the method of finding the zero of the Wronskian in the case of AdS has great accuracy due to the asymptotic decay of the regular solutions.

## 2. The Horowitz-Hubeny method

One can also apply the Horowitz-Hubeny numerical method to the Proca equations in  $d$ -dimensions. This method is well suited for determining QNMs in asymptotically AdS spacetimes and has become one of the standard approaches for studying perturbations in such backgrounds. Although the method has been clearly described in several works in the literature, for completeness we provide a brief review of its implementation in Appendix A. We have compared the results of the two methods we use.

### B. Numerical integration methods for the Maxwell field: Decoupled equations

The numerical integration shooting method to obtain the QNMs for the Maxwell field in  $d$  dimensions is based on integrating the Schrödinger-like equation also starting

from a point near the horizon, with radius  $r_i = r_h(1 + \epsilon)$ ,  $\epsilon \ll 1$ . Since the boundary condition at the horizon for Maxwell field perturbations is the same as for Proca field perturbations, i.e., it is given by Eq. (30), the method for decoupled equations apply straightforwardly here. One expands  $u_{12}$  and  $u_3$  of Eqs. (19) and (26), respectively in the same way as we did for the Proca field in Eqs. (57) and (58) and numerically find the functions.

For the Maxwell field in  $d$  dimensions one can also apply the Horowitz-Hubeny method and compare it as we did with the shooting method specified above.

## VI. NUMERICAL ANALYSIS OF THE PROCA AND MAXWELL QUASINORMAL MODES

### A. Numerical parameters

We now proceed with the presentation and the analysis of the numerical results for the QNMs. The numerical results of this section were obtained using the integration methods outlined in Sec. V. The shooting method has proven to be highly reliable for computing the QNMs, as the boundary conditions imposed require one to minimize the dominating piece of the solution at spatial infinity. When feasible, the results were cross-checked with the Horowitz-Hubeny method, see also Sec. V and Appendix A. However, the Horowitz-Hubeny method suffers from some subtleties. Namely, for sufficiently small black holes, typically  $\frac{r_h}{l} \leq 0.5$ , the method's convergence properties worsen, leading to increased computing time and numerical error contamination. Moreover, the Frobenius series, see Eq. (A4), is only applicable if the region of interest,  $x \in (0, x_h]$ , lies within the series' radius of convergence. While it can be shown that this condition is satisfied for large black holes and  $d \leq 7$ , such cannot be assured for smaller black holes or higher dimensions.

For the numerical integration, we have used  $N_i = N_f = 6$  for the order of the expansions near the horizon and in the far region. We have fixed the near-horizon radius to be  $r_i = 1.01r_h$ , i.e.,  $\epsilon = 0.01$ , and the far region radius  $r_f = 10^{11}r_h$ , i.e.,  $\kappa = 10^{11}$ . The intermediate radius at which we minimize the Wronskian was set at  $r_m = 0.67r_f$ . A reasonable variation in these values gives the same results within our precision. The numerical tool used to integrate the differential equations was *NDSolve* and the numerical tool used to find the root of the Wronskian was *FindRoot* from *Mathematica*.

### B. General characterization of the quasinormal mode frequency spectrum

We establish the parameter space for the QNMs and conduct a detailed analysis of their properties across various regions within this space. In Schwarzschild-AdS spacetime, there are two different length scales: the radius of the black hole,  $r_h$ , and the radius of curvature

of AdS,  $l$ . The Schrödinger-like equations are invariant under a rescaling on  $r$ ,  $\mu$ , and  $\omega$ , which corresponds to choosing the units of the physical quantities. In particular, one can perform the rescaling  $r \rightarrow \frac{r}{l}$ ,  $\omega \rightarrow \omega l$ ,  $\mu \rightarrow \mu l$ , so that the equations are independent of  $l$ . Thus, without loss of generality, in the numerical results we fix  $l = 1$ .

In asymptotically AdS spacetimes, the qualitative behavior of the QNM spectrum highly depends on the radius of the black hole [33, 34, 36], so it is useful to do a separate study for three different types of black holes, according to their radii: large black holes, with  $\frac{r_h}{l} \gg 1$ , intermediate black holes, with  $\frac{r_h}{l} \simeq 1$ , and small black holes, with  $\frac{r_h}{l} \ll 1$ . In addition, the QNM spectrum depends on the dimension  $d$  of the spacetime as well as on the perturbation-related parameters: the type of perturbation, either scalar-type and vector-type, the mass of the field,  $\mu$ , the angular momentum number,  $\ell$ , and the overtone number,  $k$ . Our analysis focuses on 4, 5, 6, 7-dimensional Schwarzschild-AdS spacetimes, generalization to other higher dimensions can be made.

In order to interpret correctly the spectrum for scalar-type Proca perturbations, we make the distinction between the two modes described by the coupled system Eq. (13). For that, we define two polarizations. One is the nonelectromagnetic polarization, which contains the physical degree of freedom of the monopole mode of the Proca field and reduces to the pure-gauge degree of freedom in the electromagnetic limit. Indeed, Eq. (25) allows us to interpret the nonelectromagnetic polarization as a scalar field polarization. The other is the electromagnetic polarization, which corresponds to the physical degree of freedom in the electromagnetic limit. Assuming that the QNMs change smoothly when the field acquires mass, it is expected that the nonelectromagnetic and electromagnetic polarization modes approach those of scalar field perturbations and scalar-type Maxwell perturbations, respectively, in the small-mass limit with a fixed  $r_h$ . However, such behavior does not happen in the case of  $d = 4$ , as we shall see below. We note a difference in the nomenclature “scalar-type” and “vector-type” adopted in [19, 50] with the one used here. In [19, 50], the “scalar-type” and “vector-type” polarizations were motivated by their mode behavior, i.e., “scalar-type” behaves as a scalar field and “vector-type” behaves as a vector field, and correspond to our scalar-type nonelectromagnetic polarization and vector-type/scalar-type electromagnetic polarizations, respectively. However, the nomenclature adopted in [19, 50] to distinguish between the two polarizations only makes sense in  $d = 4$ , where the scalar-type and vector-type Maxwell modes are exactly isospectral. In higher-dimensional spacetimes, isospectrality no longer happens, making the aforementioned nomenclature unsuitable.

We present in Fig. 1 some of the numerical results we have worked out, specifically, the fundamental QNM frequencies of  $\ell = 1$  scalar-type with electromagnetic polarization (asterisks), vector-type (squares), and scalar-type

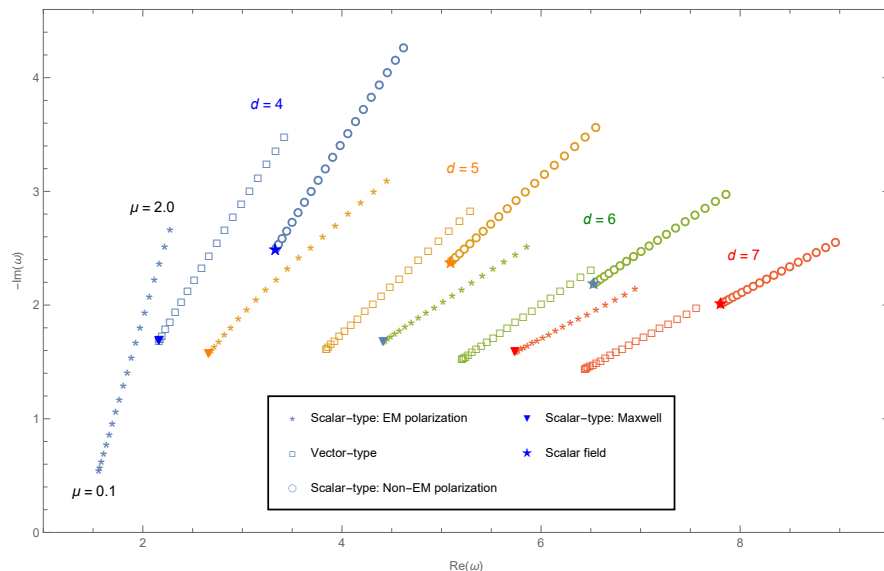


FIG. 1. Fundamental QNM frequencies of  $\ell = 1$  scalar-type with electromagnetic polarization (asterisks), vector-type (squares), and scalar-type with nonelectromagnetic polarization (circles), Proca perturbations with field masses  $\mu = 0.1, 0.2, \dots, 2.0$ , in a  $r_h = 1$  Schwarzschild-AdS black hole with  $d = 4$  (blue),  $d = 5$  (orange),  $d = 6$  (green), and  $d = 7$  (red), spacetime dimensions. Scalar-type Maxwell (triangles) and scalar field (stars) QNM frequencies are also plotted.

with nonelectromagnetic polarization (circles), Proca perturbations with field masses  $\mu = 0.1, 0.2, \dots, 2.0$ , in a  $r_h = 1$  Schwarzschild-AdS black hole with  $d = 4$  (blue),  $d = 5$  (orange),  $d = 6$  (green), and  $d = 7$  (red), spacetime dimensions. Scalar-type Maxwell (triangles) QNM frequencies are also shown. To be complete scalar field (stars) QNM frequencies are also plotted. The scalar fields  $\phi$  obey the scalar equation  $\mathcal{D}_\ell^{s=0}\phi = 0$ , where  $\mathcal{D}_\ell^{s=0}$  is the operator defined in Eq. (22).

To complete these results we present the numerical results of the fundamental QNM frequencies in four tables in the Appendix B for the typical range of the parameters in the literature, namely for 4, 5, 6, 7-dimensional Schwarzschild-AdS black holes with radius  $r_h \in [0.05, 1, 100]$  and Proca mass  $\mu \in [0, 0.1, 0.2, 0.3, 0.4, 0.5]$ . Generically, the QNM frequencies increase with the dimension and with the Proca mass in these ranges.

### C. Analysis of the dependence of the quasinormal modes on the Proca field mass

We now give a specific analysis of the dependence of the QNM frequencies on the Proca field mass. In Fig. 1 it is shown the effect of the mass of the field on the  $\ell = 1$  QNMs for 4, 5, 6, 7-dimensional Schwarzschild-AdS black holes with size  $r_h = 1$ . For all spacetime dimensions, both real and imaginary parts of the frequencies increase in magnitude with increasing mass, in agreement with what was found for  $d = 4$  in [16, 50]. The increase of the real part is related to the decrease of the Compton wavelength of the Proca particle,  $\lambda_c = \frac{1}{\mu}$ . On the other hand, the increase of the imaginary part is a consequence of the

barrier becoming less pronounced with increasing mass. Note that such effect on the QNMs is suppressed for higher-dimensional spacetimes, as these already provide a mass term to the potential, i.e.,  $\mu_{\text{eff}}^2 = \mu^2 + \frac{(d-2)(d-4)}{4l^2}$ .

For  $d \geq 5$ , the scalar-type Proca modes with electromagnetic polarization reach, in the massless limit, the scalar-type Maxwell modes. Such does not happen, however, for  $d = 4$ : in this case, the scalar-type and vector-type sectors are isospectral, and the transition from massless to massive regimes is not smooth. Indeed, for  $\mu = 0$ , we have  $\mu_{\text{eff}} = 0$ , and the potential does not diverge at infinity, whereas for  $\mu > 0$ , we have  $\mu_{\text{eff}} > 0$ , and the potential diverges. This discontinuity is visible in Fig. 1 already for  $\mu = 0.1$ . The analysis is not done for smaller mass, because the method with the coupled system gives results dependent on the initialization of *FindRoot*, which indicates a failure of accuracy of the method.

Lastly, note from the figure that scalar-type Proca modes with nonelectromagnetic polarization reach the scalar field modes, in the massless limit and for all spacetime dimensions, in agreement with Eq. (25).

### D. Analysis of the dependence of the quasinormal modes on the black hole radius

#### 1. Large black holes

##### (a) Ordinary modes of large black holes

We now analyze the dependence of the QNMs on large black hole horizon radius for ordinary modes. As shown

in [31], the ordinary modes are QNMs in which their frequencies for large Schwarzschild-AdS black holes should scale linearly with the radius of the black hole, i.e.,  $\omega \sim r_h$ . The results for scalar-type Proca perturbations and for vector-type Proca perturbations are similar.

In Fig. 2 the results for the real part of the QNM frequencies of  $\ell = 1$  vector-type Proca perturbations in 5, 6, 7-dimensional Schwarzschild-AdS black holes, as a function of the black hole radius, in the large black hole regime, are displayed. The scaling of the frequency  $\omega$  with the horizon radius  $r_h$  appears in a clear way.

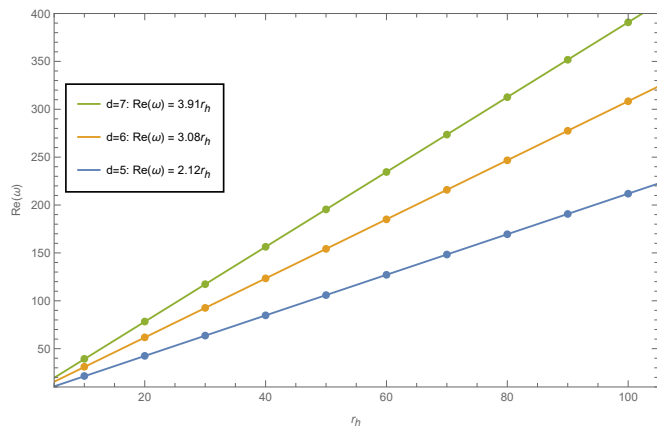


FIG. 2. Real part of the QNM frequencies of  $\ell = 1$ ,  $\mu = 0.5$ , vector-type Proca perturbations in 5, 6, 7-dimensional Schwarzschild-AdS black holes, as a function of the black hole radius, in the large black hole regime. Ordinary modes scale linearly with the radius of the black hole.

In Tables I and II we show the fundamental QNM frequencies of  $\ell = 1$  scalar-type and vector-type Proca perturbations and  $\ell = 1$  scalar-type and vector-type Maxwell perturbation in  $d = 7$  large Schwarzschild-AdS black holes, respectively. For Proca perturbations, Table I displays isospectrality between the electromagnetic polarized scalar-type modes and the vector-type modes in the limit of very large  $r_h$ , although we have not found an analytical proof for this statement. For Maxwell perturbations, the isospectrality between the two sectors is clearly displayed in Table II in the limit of very large  $r_h$ , in agreement with the analytical proof of Section IV C.

$r_h$	$\omega$ (Scalar-type, NonEM)	$\omega$ (Scalar-type, EM)	$\omega$ (Vector-type)
500	2638.34 – 1390.90i	2054.37 – 1083.43i	2054.37 – 1083.43i
250	1319.18 – 695.448i	1027.19 – 541.716i	1027.20 – 541.715i
100	527.702 – 278.173i	410.897 – 216.682i	410.906 – 216.680i
50	263.902 – 139.076i	205.484 – 108.334i	205.502 – 108.330i
25	132.054 – 69.5159i	102.813 – 54.1533i	102.849 – 54.1441i
10	53.1090 – 27.7452i	41.3223 – 21.6225i	41.4135 – 21.5997i

TABLE I. Fundamental QNMs of  $\mu = 1$  Proca  $\ell = 1$  perturbations in  $d = 7$  large Schwarzschild-AdS black holes. For large black holes, scalar-type nonelectromagnetically polarized stand apart, whereas scalar-type electromagnetically polarized perturbations and vector-type Proca perturbations tend to isospectrality.

$r_h$	$\omega$ (Scalar-type)	$\omega$ (Vector-type)
500	1918.30 – 999.501i	1918.30 – 999.501i
250	959.155 – 499.749i	959.159 – 499.748i
100	383.681 – 199.896i	383.691 – 199.894i
50	191.875 – 99.9413i	191.894 – 99.9367i
25	96.0056 – 49.9572i	96.0447 – 49.9481i
10	38.5930 – 19.9454i	38.6901 – 19.9228i

TABLE II. Fundamental QNMs of Maxwell  $\ell = 1$  perturbations in large  $d = 7$  Schwarzschild-AdS black holes. For sufficiently large black holes, the scalar-type and vector-type sectors of Maxwell perturbations are isospectral, in agreement with the analytical study of Section IV C.

### (b) Purely damped modes of large black holes

In addition to the ordinary modes, we have analyzed numerically the purely damped modes of Proca perturbations. In Fig. 3, we present the results for Proca scalar perturbations in 7-dimensional large Schwarzschild-AdS black holes, as a function of the black hole radius. Purely damped modes of Proca perturbations scale linearly with the black hole radius as shown. We have not pursued an analytic study of Proca perturbations, as this would require solving the coupled system given in Eq. (13). Thus, further investigation is needed, but our numerical results indicate that, when the field acquires mass, the low-frequency modes start to scale linearly with the black hole radius as indicated in the figure.

In addition to the ordinary modes, we have as well analyzed numerically the purely damped modes of Maxwell perturbations. In Fig. 4, we present the results for  $\ell = 1, 2$  Maxwell perturbations in  $d = 5, 6, 7$  dimensions. The numerical results confirm our analytic procedure of Sec. IV D that scalar-type Maxwell perturbations in  $d \geq 5$  large Schwarzschild-AdS black holes exhibit purely damped QNM frequencies scaling linearly with the inverse of the radius. Furthermore, no purely damped modes were found for scalar-type perturbations in  $d = 4$  Schwarzschild-AdS black holes, neither for vector-type perturbations in all spacetime dimensions, once again confirming the results of Sec. IV D.

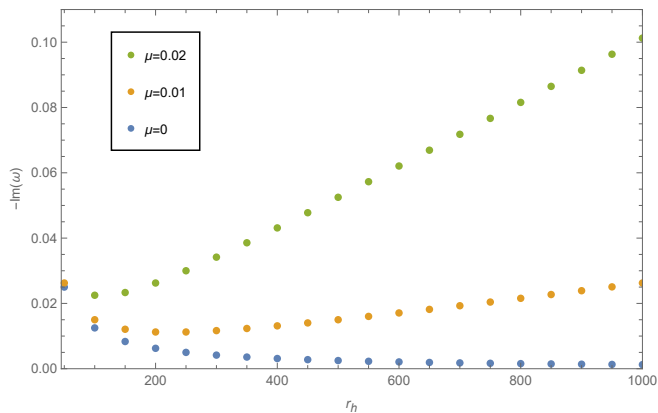


FIG. 3. Purely damped modes of  $\mu = 0.01$  Proca (orange), and  $\mu = 0.02$  Proca (green),  $\ell = 1$  scalar-type perturbations in 7-dimensional large Schwarzschild-AdS black holes are plotted as a function of the black hole radius. Purely damped modes of Proca perturbations scale linearly with the black hole radius. Purely damped modes of Maxwell (blue) scalar-type perturbations in 7-dimensional large Schwarzschild-AdS black holes are plotted as a function of the black hole radius. Purely damped modes of Maxwell perturbations scale linearly with the inverse of the radius, in contrast with Proca modes.

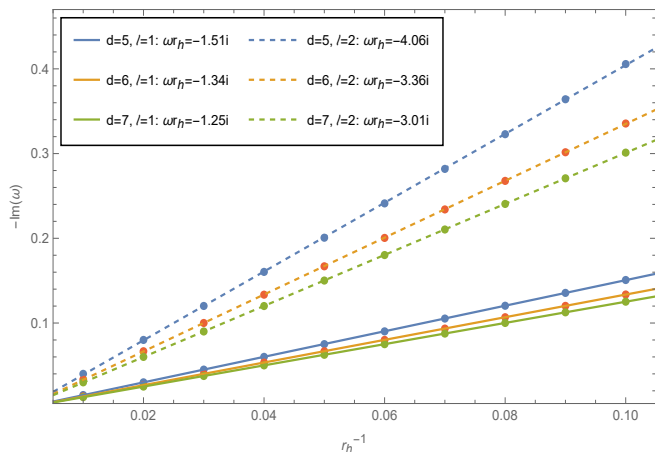


FIG. 4. Purely damped modes of scalar-type Maxwell  $\ell = 1$  (solid lines) and  $\ell = 2$  (dashed lines) perturbations in 5-dimensional (blue), 6-dimensional (orange), and 7-dimensional (green), large Schwarzschild-AdS black holes, as a function of the inverse of the black hole radius. The numerical results show support for Eq. (53). Note the linear scaling with  $r_h^{-1}$ .

### 2. Intermediate black holes

We now analyze the case of intermediate black holes. As we decrease the horizon radius from the large black hole case, the QNMs start to deviate from the linear scaling as one approaches  $r_h \simeq 1$ . This is shown in Fig. 5, where it can be seen that the real part of the frequencies approaches a minimum for  $r_h < 1$ , meaning that there are differently-sized black holes having QNM frequencies

with the same real part. This may be due to the fact

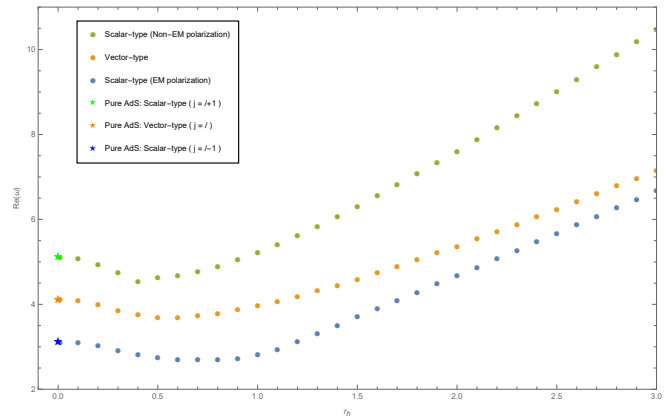


FIG. 5. Real part of the fundamental QNM frequencies of  $\ell = 1$ ,  $\mu = 0.5$ , scalar-type with electromagnetic polarization (blue), vector-type (orange), and scalar-type with nonelectromagnetic polarization (green) Proca perturbations in 5-dimensional intermediate and small Schwarzschild-AdS black holes plotted as a function of the black hole radius. The pure AdS normal mode frequencies (stars) were also plotted [54].

that the black hole starts to have a comparable size with the Compton wavelength of the field,  $\lambda_c = \frac{1}{\omega}$ .

### 3. Small black holes

We now analyze the case of small black holes. As one approaches the  $r_h \rightarrow 0$  limit, the QNM frequencies approach those of pure AdS spacetime, see Fig. 5, studied in [54]. Scalar-type Proca modes with nonelectromagnetic and electromagnetic polarizations approach the scalar-type  $j = \ell + 1$  and the scalar-type  $j = \ell - 1$  modes of pure AdS, respectively, where  $j$  stands for the total angular momentum number of the modes. Likewise, vector-type Proca modes approach the vector-type  $j = \ell$  modes of pure AdS. On the other hand, as one approaches the  $r_h \rightarrow 0$  limit, the imaginary part of the frequencies starts decreasing as an  $\ell, d$ -dependent power of  $r_h$ , which is difficult to determine numerically, due to the poor convergence properties of the methods for very small black holes. An analytical approach for small black holes is done further below using matched asymptotic expansions. The vanishing of the imaginary part for very small black holes is intuitively clear, since the modes only decay due to the presence of the black hole and there is no energy dissipated through spatial infinity. However, the fact that the frequencies approach those of pure AdS was not necessarily expected, because the purely ingoing boundary condition at  $r = r_h$  in the  $r_h \rightarrow 0$  limit does not reduce to the regularity boundary condition imposed at the origin of pure AdS in [54]. Such is in accordance, however, with results for other types of perturbations [36].

## VII. MATCHED ASYMPTOTIC EXPANSIONS FOR SMALL SCHWARZSCHILD-ADS BLACK HOLES

### A. Preamble

Both the numerical shooting integration method and the Horowitz-Hubeny method begin to fail for sufficiently small black holes. In this section, we investigate if an analytical procedure for such cases can be developed, following [15, 19, 42, 47]. We do not fix the AdS length  $l$  here, as it is important for the approximations that we are taking.

The spacetime is separated initially into two different regions: the near region, the region near the black hole horizon, verifying  $\frac{r-r_h}{l} \ll \frac{1}{\omega l}$ , where the AdS curvature may be neglected, and the far region, the region far from the black hole horizon, verifying  $\frac{r-r_h}{l} \gg \frac{r_h}{l}$ , where the effect of the black hole may be neglected. The regime we work is the small black hole case, i.e.,  $\frac{r_h}{l} \ll 1$ , and the large wavelength perturbation mode approximation, i.e., small wave frequency  $\omega$  approximation,  $\omega r_h \ll 1$ . After imposing the usual boundary conditions at the horizon and at spatial infinity, the QNM frequencies are determined from the matching condition of the two solutions in the overlap region, defined through  $\frac{r_h}{l} \ll \frac{r-r_h}{l} \ll \frac{1}{\omega l}$ . Thus in brief there are three regions, namely,

$$\frac{r-r_h}{l} \ll \frac{1}{\omega l}, \quad \text{near region}, \quad (63)$$

$$\frac{1}{\omega l} \gg \frac{r-r_h}{l} \gg \frac{r_h}{l}, \quad \text{overlap region}, \quad (64)$$

$$\frac{r_h}{l} \ll \frac{r-r_h}{l}, \quad \text{far region}. \quad (65)$$

In the regime given by Eqs. (63)-(65), scalar-type Proca perturbations with  $\ell = 0$ , i.e., monopole perturbations, have decoupled equations and thus the monopole case can be handled through a matching asymptotic expansion technique. The same happens for the vector-type Proca perturbations. Indeed, for monopole and vector-type Proca perturbations, the associated decoupled Schrödinger-like equations can be solved analytically in each region and then overlapped. Maxwell perturbations can also be handled in this regime. On the other hand for this regime, i.e., the regime given by Eqs. (63)-(65), the coupled modes associated to  $\ell \geq 1$  scalar-type Proca perturbations remain nontrivially coupled in the near region, and for such perturbations it is not possible to perform a matching of the solutions.

In what follows, we study the scalar monopole and vector-type Proca perturbations in  $d$  dimensions. We also do the matching of the Maxwell field in  $d$  dimensions which has not been previously done.

### B. Proca perturbations: Matched asymptotic expansions in the scalar monopole and vector-type cases

#### 1. Scalar-type Proca perturbations: Monopole case

##### Near region

To deal with the near region we define the unitless radial coordinate  $z$  by

$$z \equiv z(r) = 1 - \left(\frac{r_h}{r}\right)^{d-3}, \quad (66)$$

meaning  $z = 0$  at the horizon and  $z = 1$  at spatial infinity. From Eq. (7) together with Eq. (15), the  $\ell = 0$  Schrödinger-like equation in the near region is then

$$\begin{aligned} z(1-z) \frac{d^2 u_1^{\text{near}}}{dz^2} + \left(1-z \left(2 + \frac{1}{d-3}\right)\right) \frac{du_1^{\text{near}}}{dz} + \frac{1}{(d-3)^2} \left(\frac{\omega^2 r_h^2}{z(1-z)} - \frac{\mu^2 r_h^2}{1-z}\right) u_1^{\text{near}} - \frac{d(d-2)z}{4(1-z)} + \frac{(d-2)(d-3)}{2} u_1^{\text{near}} = 0, \end{aligned} \quad (67)$$

where we assume that  $\mu(r-r_h) \ll 1$  for some Proca mass  $\mu$  and so this term can be neglected, as we only consider leading order terms in  $r_h$ , but keep the term  $\omega r_h$ . The solution to Eq. (67) is given by the Gaussian hypergeometric function  ${}_2F_1$  [59] as  $u_1^{\text{near}}(z) = cz^{-i\bar{\omega}} (1-z)^{\frac{d-2}{2(d-3)}} {}_2F_1 \left[2 + \frac{2}{d-3} - i\bar{\omega}, -i\bar{\omega}; 1 - 2i\bar{\omega}; z\right]$ , for some constant  $c$  and  $\bar{\omega} \equiv \frac{\omega r_h}{d-3}$ .

The near region solution in the overlap region for  $d \geq 6$  is

$$u_1^{\text{near}} = ca_1^{\text{near}} \left(\frac{r}{r_h}\right)^{-\frac{d-2}{2}} + cb_1^{\text{near}} \left(\frac{r}{r_h}\right)^{\frac{d}{2}}, \quad (68)$$

$$\begin{aligned} a_1^{\text{near}} &= \frac{\Gamma[1-2i\bar{\omega}]\Gamma[-1-\frac{2}{d-3}]}{\Gamma[1-i\bar{\omega}]\Gamma[-1-\frac{2}{d-3}-i\bar{\omega}]}, \\ b_1^{\text{near}} &= \frac{\Gamma[1-2i\bar{\omega}]\Gamma[1+\frac{2}{d-3}]}{\Gamma[2+\frac{2}{d-3}-i\bar{\omega}]\Gamma[-i\bar{\omega}]}, \end{aligned} \quad (69)$$

with  $c = \text{constant}$ . The ratio between the coefficients from the near region solution is

$$\frac{a_1^{\text{near}} r_h^{d-1}}{b_1^{\text{near}}} = -\frac{1 + \frac{2}{d-3}}{i\bar{\omega}} r_h^{d-1}, \quad (70)$$

where we have used that  $\Gamma[1-i\bar{\omega}] = -i\bar{\omega}\Gamma[-i\bar{\omega}]$  and we have neglected the contribution of  $\bar{\omega}$  in the remaining  $\Gamma$ 's. While the expression in Eq. (70) seems to be formally valid only for  $d \geq 6$ , it is also valid for  $d = 4$  and  $d = 5$ . For these specific cases, one must use the correct transformation to obtain the behavior at the overlap region. This yields a leading order term containing a logarithm. However, the dominant term is  $\psi[-i\bar{\omega}]$ , where  $\psi[x]$  is the

digamma function, i.e.,  $\psi[x] = \frac{d(\ln \Gamma[x])}{dx}$ . It diverges for  $\omega r_h \ll 1$  but can be regularized by  $\frac{1}{\Gamma[-1-\frac{1}{d-3-i\omega}]}$ . The resulting asymptotic behavior yields the same as Eq. (68) with the coefficient ratio given by Eq. (70).

#### Far region

To deal with the far region we define the unitless radial coordinate  $y$  as

$$y \equiv y(r) = \left(1 + \frac{r^2}{l^2}\right)^{-1}, \quad (71)$$

such that  $y = 0$  at spatial infinity and  $y = 1$  at the event horizon.

Using the approximation  $\frac{r-r_h}{l} \gg \frac{r_h}{l}$  and Eq. (7) with  $\ell = 0$  and  $u_2 = 0$ , we can obtain the Proca perturbation equation for  $u_1$  in the far region regime. It is

$$\begin{aligned} y(1-y) \frac{\partial^2 u_1^{\text{far}}}{\partial y^2} + \left(\frac{1}{2} - y\right) \frac{\partial u_1^{\text{far}}}{\partial y} \\ + \left(\frac{\omega^2 l^2}{4} - \frac{(d-2)d}{16(1-y)}\right. \\ \left. - \frac{1}{4y} \left(\mu^2 l^2 + \frac{(d-4)(d-2)}{4}\right)\right) u_1^{\text{far}} = 0. \end{aligned} \quad (72)$$

The solution of Eq. (72) obeying the Dirichlet boundary condition at  $y = 0$  is  $u_1^{\text{far}}(y) = cy^{\frac{1}{4}(2\gamma-1)}(1-y)^{\frac{d}{4}} {}_2F_1[\eta_1, \sigma_1; \gamma; y]$ , for some constant  $c$ , with  $\eta_1 = \frac{1}{4}(2\gamma + d - 1 + 2\omega l)$ ,  $\sigma_1 = \frac{1}{4}(2\gamma + d - 1 - 2\omega l)$ ,  $\gamma = 1 + \frac{1}{2}\sqrt{(d-3)^2 + 4\mu^2 l^2}$ .

Using the linear transformation law of the hypergeometric function  $y \rightarrow 1 - y$ , the behavior in the overlap region of the solution of Eq. (72) for noninteger  $\gamma - \eta_1 - \sigma_1 = -\frac{d-1}{2}$ , i.e., for even  $d$  is

$$u_1^{\text{far}}(r) = ca_1^{\text{far}} \left(\frac{r}{l}\right)^{-\frac{d-2}{2}} + cb_1^{\text{far}} \left(\frac{r}{l}\right)^{\frac{d}{2}}, \quad (73)$$

$$a_1^{\text{far}} = \frac{\Gamma[\eta_1 + \sigma_1 - \gamma]}{\Gamma[\eta_1]\Gamma[\sigma_1]}, \quad b_1^{\text{far}} = \frac{\Gamma[\gamma - \eta_1 - \sigma_1]}{\Gamma[\gamma - \eta_1]\Gamma[\gamma - \sigma_1]}. \quad (74)$$

The ratio between the coefficients for the far region solution in the overlap region is

$$\frac{a_1^{\text{far}} l^{d-1}}{b_1^{\text{far}}} = -\frac{k! \Gamma[\frac{d-1}{2}] \Gamma[k + \gamma] i \delta l^d}{2\Gamma[\gamma + k + \frac{d-1}{2}] (\frac{d+1}{2})_k}, \quad (75)$$

where the QNM frequency was expanded as  $\omega = \omega_{\text{AdS}} + i\delta$  and only leading order in  $|\delta| \ll \omega_{\text{AdS}}$  was considered, with  $\omega_{\text{AdS}} l = \gamma + 2k + \frac{d-1}{2}$ ,  $k$  being the overtone number and a non-negative integer, and where  $(x)_n \equiv \frac{\Gamma[x+n]}{\Gamma[x]}$  is the Pochhammer symbol for a real number  $x$ . In order to obtain the expression in Eq. (75), we have used that, for an integer  $k$  and a small  $\delta$ ,  $\lim_{z \rightarrow -k} \frac{1}{\Gamma[z+i\delta]} = (-1)^k k! i\delta$  and also  $\Gamma[z+i\delta] = \Gamma[z]$  for noninteger  $z$ .

#### Overlap region

The matching of the two solutions in the overlap region is performed by equating the ratio in Eq. (70) with the ratio in Eq. (75), i.e.,  $\frac{a_1^{\text{near}} r_h^{d-1}}{b_1^{\text{near}}} = \frac{a_1^{\text{far}} l^{d-1}}{b_1^{\text{far}}}$ . The real part of the correction to the QNMs, i.e.,  $\delta l$ , for the monopole case is

$$\begin{aligned} \Re \delta = -\frac{2(d-1)\Gamma[\frac{d-1}{2} + k + \gamma]}{k! \Gamma[\frac{d-1}{2}] \Gamma[k + \gamma]} \left(\frac{d+1}{2}\right)_k \\ \times \left(\frac{r_h}{l}\right)^{d-2} \frac{1}{\omega_{\text{AdS}}}. \end{aligned} \quad (76)$$

Note that  $\delta$  scales linearly with the inverse of the pure AdS frequency, whereas for the vector-type perturbation, as we will see, it scales linearly with the pure AdS frequency. Also,  $\Re \delta \sim \left(\frac{r_h}{l}\right)^{d-2}$ , which is useful for comparison with the numerical results, as can be seen in Tables III and IV. Note that the agreement between numerical and analytical results for monopole perturbations is highly satisfactory. Indeed, since the monopole frequencies decrease slowly with the radius of the black hole, we were able to obtain numerical results for small black holes, for which the approximations of the analytical method are good.

	$k$	$\mu$	$\Re \delta_n l$	$\Re \delta_a l$
$d = 4$	0	0.5	$-5.66689 \times 10^{-8}$	$-5.66321 \times 10^{-8}$
	0	2.0	$-8.88933 \times 10^{-8}$	$-8.88073 \times 10^{-8}$
	1	0.5	$-1.64019 \times 10^{-7}$	$-1.63822 \times 10^{-7}$
$d = 5$	0	0.5	$-1.28297 \times 10^{-11}$	$-1.28296 \times 10^{-11}$
	0	2.0	$-2.09443 \times 10^{-11}$	$-2.09443 \times 10^{-11}$
	1	0.5	$-5.03700 \times 10^{-11}$	$-5.03698 \times 10^{-11}$

TABLE III. Comparison between numerical results for the real part of  $\delta l$ ,  $\Re \delta_n l$ , and analytical results obtained from Eq. (76),  $\Re \delta_a l$ , for different parameters of the monopole Proca perturbation in  $d = 4, 5$  Schwarzschild-AdS black holes, with radius  $\frac{r_h}{l} = 10^{-4}$ .

	$k$	$\mu$	$\Re \delta_n l$	$\Re \delta_a l$
$d = 6$	0	0.5	$-2.30944 \times 10^{-9}$	$-2.30877 \times 10^{-9}$
	0	2.0	$-3.66837 \times 10^{-9}$	$-3.66693 \times 10^{-9}$
	1	0.5	$-1.14208 \times 10^{-8}$	$-1.14145 \times 10^{-8}$
$d = 7$	0	0.5	$-1.51407 \times 10^{-11}$	$-1.51388 \times 10^{-11}$
	0	2.0	$-2.30083 \times 10^{-11}$	$-2.30046 \times 10^{-11}$
	1	0.5	$-9.01694 \times 10^{-11}$	$-9.01485 \times 10^{-11}$

TABLE IV. Comparison between numerical results for the real part of  $\delta l$ ,  $\Re \delta_n l$ , and analytical results obtained from Eq. (76),  $\Re \delta_a l$ , for different parameters of the monopole Proca perturbation in  $d = 6, 7$  Schwarzschild-AdS black holes, with radius  $\frac{r_h}{l} = 3 \times 10^{-3}$ .

## 2. Vector-type Proca perturbations

### Near region

In the near region, the background is essentially Schwarzschild, and one can use the approximation  $\frac{r-r_h}{l} \ll \frac{1}{\omega l}$  to rewrite Eq. (11) as

$$z(1-z) \frac{d^2 u_3^{\text{near}}}{dz^2} + \left(1 - z \left(2 + \frac{1}{d-3}\right)\right) \frac{du_3^{\text{near}}}{dz} + \frac{1}{(d-3)^2} \left( \frac{\omega^2 r_h^2}{z(1-z)} - \frac{(\ell+1)(\ell+d-4) + \mu^2 r_h^2}{1-z} - \frac{(d-4)(d-6)z}{4(1-z)} - \frac{(d-4)(d-3)}{2} \right) u_3^{\text{near}} = 0, \quad (77)$$

with  $z \equiv z(r) = 1 - \left(\frac{r_h}{r}\right)^{d-3}$ , see Eq. (66), meaning  $z = 0$  at the horizon and  $z = 1$  at spatial infinity, and where it was assumed that, in the near region,  $\mu(r - r_h) \ll 1$ . Moreover, the term  $\mu r_h \ll 1$  may be neglected, since it provides a minor correction to  $(\ell+1)(\ell+d-4) \gtrsim 1$ . The solution to Eq. (77) obeying the ingoing boundary condition, Eq. (28), at  $z = 0$ , is given in terms of the Gaussian hypergeometric function  ${}_2F_1$  [59] as  $u_3^{\text{near}} = cz^{-i\bar{\omega}}(1-z)^{\frac{2\ell+d-4}{2(d-3)}} {}_2F_1\left[1 + \frac{\ell-1}{d-3} - i\bar{\omega}, 1 + \frac{\ell+1}{d-3} - i\bar{\omega}; 1 - 2i\bar{\omega}; z\right]$ , for some constant  $c$ , with  $\bar{\omega} \equiv \frac{\omega r_h}{d-3}$ .

One now must obtain the functional behavior of the near region solution in the overlap region, by performing the transformation  $z \rightarrow 1 - z$  of the hypergeometric function and consider the leading order terms of  $\frac{r_h}{r} \ll 1$ . However, one must be careful to do such transformation as its validity depends on whether  $-1 - \frac{2\ell}{d-3}$  is an integer or not, i.e., whether  $\frac{2\ell}{d-3}$  is an integer or not. For a noninteger  $\frac{2\ell}{d-3}$ , we have at the overlap region

$$u_3^{\text{near}}(r) = ca_3^{\text{near}} \left(\frac{r}{r_h}\right)^{-\frac{2\ell+d-4}{2}} + cb_3^{\text{near}} \left(\frac{r}{r_h}\right)^{\frac{2\ell+d-2}{2}}, \quad (78)$$

$$a_3^{\text{near}} = \frac{\Gamma[-1 - \frac{2\ell}{d-3}]}{\Gamma[-\frac{\ell-1}{d-3} - i\bar{\omega}]\Gamma[-\frac{\ell+1}{d-3} - i\bar{\omega}]}, \quad (79)$$

$$b_3^{\text{near}} = \frac{\Gamma[1 + \frac{2\ell}{d-3}]}{\Gamma[1 + \frac{\ell-1}{d-3} - i\bar{\omega}]\Gamma[1 + \frac{\ell+1}{d-3} - i\bar{\omega}]}. \quad (80)$$

From the definition of the near region, Eq. (78) holds approximately in the region  $0 \ll r - r_h \ll \frac{1}{\omega}$ . To perform the matching, the relevant quantity is in fact the ratio between the coefficients of the two leading terms. This is because one can always absorb a common factor into the constant  $c$ . We have for small  $\bar{\omega}$  and noninteger  $\frac{2\ell}{d-3}$

$$\frac{a_3^{\text{near}} r_h^{2\ell+d-3}}{b_3^{\text{near}}} = \frac{\Gamma^2[1 + \frac{\ell-1}{d-3}]\Gamma^2[1 + \frac{\ell+1}{d-3}]r_h^{2\ell+d-3}}{(1 + \frac{2\ell}{d-3})\Gamma^2[1 + \frac{2\ell}{d-3}]} \times \left( \frac{\sin\left(\frac{\pi(\ell-1)}{d-3}\right)\sin\left(\frac{\pi(\ell+1)}{d-3}\right)}{\pi \sin\left(\frac{2\ell\pi}{d-3}\right)} + i\bar{\omega} \right), \quad (81)$$

where the equality is approximate. For integer  $\frac{2\ell}{d-3}$ , i.e., for  $-1 - \frac{2\ell}{d-3} \equiv -m$ , where  $m$  is a positive integer, then  $a_3^{\text{near}}$  diverges, Eq. (78) is not valid, and the upshot is that it is not possible to make the matching. Indeed, in this case, one must take the correct transformation [59] giving the leading terms  $\left(\frac{r}{r_h}\right)^{\frac{2\ell+d-2}{2}}$  and  $\frac{1}{\Gamma[-\frac{\ell-1}{d-3} - i\bar{\omega}]\Gamma[-\frac{\ell+1}{d-3} - i\bar{\omega}]} \left(\frac{r}{r_h}\right)^{-\frac{2\ell+d-4}{2}} ((d-3) \ln\left(\frac{r_h}{r}\right) - \psi[1] - \psi[m+1] + \psi\left[1 + \frac{\ell-1}{d-3} - i\bar{\omega}\right] + \psi\left[1 + \frac{\ell+1}{d-3} - i\bar{\omega}\right])$ , where  $\psi[x]$  is the digamma function, i.e.,  $\psi[x] = \frac{d \ln \Gamma[x]}{dx}$ . As we are interested in  $\frac{r_h}{r} \ll 1$ , the logarithmic term dominates in the second leading order term and so the behavior of the solution for integer  $\frac{2\ell}{d-3}$  is described by  $\left(\frac{r}{r_h}\right)^{\frac{2\ell+d-2}{2}}$  and  $\left(\frac{r}{r_h}\right)^{-\frac{2\ell+d-4}{2}} \ln\left(\frac{r_h}{r}\right)$ . Thus, for this case, the functional matching is not possible as the far region does not have such asymptotic behavior.

### Far region

In the far region, the background is essentially pure AdS and the effect of the black hole can be neglected. To deal with the far region we define the unitless radial coordinate  $y$  as  $y \equiv y(r) = \left(1 + \frac{r^2}{l^2}\right)^{-1}$ , see Eq. (71), such that  $y = 0$  at spatial infinity and  $y = 1$  at the event horizon. Using the approximation  $\frac{r-r_h}{l} \gg \frac{r_h}{l}$ , Eq. (11) can be written as

$$y(1-y) \frac{\partial^2 u_3^{\text{far}}}{\partial y^2} + \left(\frac{1}{2} - y\right) \frac{\partial u_3^{\text{far}}}{\partial y} + \left(\frac{\omega^2 l^2}{4} - \frac{(2\ell+d-4)(2\ell+d-2)}{16(1-y)} - \frac{1}{4y} \left(\mu^2 l^2 + \frac{(d-4)(d-2)}{4}\right)\right) u_3^{\text{far}} = 0. \quad (82)$$

The solution of Eq. (82) obeying the Dirichlet boundary condition at  $y = 0$  is  $u_3^{\text{far}}(y) = cy^{\frac{1}{4}(2\gamma-1)}(1-y)^{\frac{2\ell+d-2}{4}} {}_2F_1[\eta_\ell, \sigma_\ell; \gamma; y]$ , for some constant  $c$ , with  $\eta_\ell = \frac{1}{4}(2\gamma + 2\ell + d - 3 + 2\omega)$ ,  $\sigma_\ell = \frac{1}{4}(2\gamma + 2\ell + d - 3 - 2\omega l)$ ,  $\gamma = 1 + \frac{1}{2}\sqrt{(d-3)^2 + 4\mu^2 l^2}$ .

One now must obtain the functional behavior of the far region solution in the overlap region. Using the linear transformation law of the hypergeometric function  $y \rightarrow 1 - y$ , the behavior of the solution in the overlap region for noninteger  $\gamma - \eta_\ell - \sigma_\ell = -\ell - \frac{d-3}{2}$ , i.e., for even  $d$  is

$$u_3^{\text{far}}(r) = ca_3^{\text{far}} \left(\frac{r}{l}\right)^{-\frac{2\ell+d-4}{2}} + cb_3^{\text{far}} \left(\frac{r}{l}\right)^{\frac{2\ell+d-2}{2}}, \quad (83)$$

$$a_3^{\text{far}} = \frac{\Gamma[\eta_\ell + \sigma_\ell - \gamma]}{\Gamma[\eta_\ell]\Gamma[\sigma_\ell]}, \quad b_3^{\text{far}} = \frac{\Gamma[\gamma - \eta_\ell - \sigma_\ell]}{\Gamma[\gamma - \eta_\ell]\Gamma[\gamma - \sigma_\ell]}, \quad (84)$$

Since one is in the AdS regime, Eq. (83) may be simplified by considering that the QNM frequencies are given by the pure AdS normal mode frequencies,  $\omega_{\text{AdS}} l = 2k + \ell + \frac{d-3}{2} + \gamma_3$ , where  $k$  is a non-negative integer, see also [54],

plus a small correction,  $\delta$ , which is complex in general. The frequencies can then be written as  $\omega = \omega_{\text{AdS}} + i\delta$ , with  $|\delta| \ll |\omega_{\text{AdS}}|$ , and the problem of finding  $\omega$  reduces to the problem of finding the correction  $\delta$ . We note that the stability study of Sec. IV B implies that  $\Re\epsilon(\delta) < 0$ . The hypergeometric coefficients become  $\eta_\ell = \gamma + k + \ell + \frac{d-3}{2} + i\frac{\delta\ell}{2}$ ,  $\sigma_\ell = -k - i\frac{\delta\ell}{2}$ ,  $\gamma - \eta_\ell = -k - \ell - \frac{d-3}{2} - i\frac{\delta\ell}{2}$ ,  $\gamma - \sigma_\ell = \gamma + k + i\frac{\delta\ell}{2}$ . With these considerations, we can now evaluate the ratio between the two leading order terms for small  $\delta$ , valid for even  $d$ , yielding

$$\frac{a_3^{\text{far}} l^{2\ell+d-3}}{b_3^{\text{far}}} = -\frac{k! \Gamma[\ell + \frac{d-3}{2}] \Gamma[k + \gamma] i \delta l^{2\ell+d-2}}{2\Gamma[\gamma + k + \ell + \frac{d-3}{2}] (1 + \ell + \frac{d-3}{2})_k}, \quad (85)$$

where  $(x)_n \equiv \frac{\Gamma[x+n]}{\Gamma[x]}$  is the Pochhammer symbol for a real number  $x$ . When  $\ell + \frac{d-3}{2} = m$ , with  $m$  being a positive integer, i.e., for odd  $d$ ,  $b_3^{\text{far}}$  diverges with  $\Gamma[\gamma - \eta_\ell - \sigma_\ell] = \Gamma[-m]$ , and the expression in Eq. (85) becomes formally invalid. In this case, one must pick the correct transformation  $y \rightarrow 1 - y$ , yielding the leading terms  $a_3^{\text{far}} (\frac{r}{l})^{-\frac{2\ell+d-4}{2}}$  and  $\frac{(-1)^{m+1}}{m! \Gamma[\gamma - \eta_\ell] \Gamma[\gamma - \sigma_\ell]} (\frac{r}{l})^{\frac{2\ell+d-2}{2}} (-2 \ln(\frac{r}{l}) - \psi[1] - \psi[m+1] + \psi[\eta_\ell] + \psi[\sigma_\ell])$ . The second leading term needs to be evaluated carefully, since  $\sigma_\ell$  and  $\gamma - \eta_\ell$  are negative integers at zeroth order in  $\delta$ . This means the logarithmic term is dropped and only the term  $\frac{\psi[\sigma_\ell]}{\gamma[\gamma - \eta_\ell]}$  survives. Using the small  $\delta$  approximation, the behavior becomes the same as Eq. (85) with integer  $\ell + \frac{d-3}{2} = m$ . Thus, the far region solution behaves as Eq. (85) for both even and odd  $d$ .

Note that the scalar monopole case follows from here, by putting  $\ell = 1$  in the vector-type perturbations. Indeed, the far region solution for the monopole perturbation in the overlap region is simply Eq. (73) with  $\ell = 1$ . Note also that in  $u_1^{\text{far}} = ca_1^{\text{far}} (\frac{r}{l})^{-\frac{d-2}{2}} + b_1^{\text{far}} (\frac{r}{l})^{\frac{d}{2}}$  of Eq. (73) the  $a_1^{\text{far}}$  and  $b_1^{\text{far}}$  are simply  $a_1^{\text{far}} = a_3^{\text{far}}|_{\ell=1}$  and  $b_1^{\text{far}} = b_3^{\text{far}}|_{\ell=1}$ , see also Eq. (84).

#### Overlap region

With the near and far region behavior in the overlap region described by  $r_h \ll r \ll \frac{1}{\omega}$ , we now proceed with the functional matching between the two regions. The previous analysis reveals that such matching is only possible for noninteger  $\frac{2\ell}{d-3}$ . Otherwise, the near region solution presents a logarithmic term in the overlap region that does not match with the expected behavior from the far-region solution. The matching condition is obtained by equating the two ratios, i.e.,  $\frac{\alpha_3^{\text{near}} r_h^{2\ell+d-3}}{b_3^{\text{near}}} = \frac{\alpha_3^{\text{far}} l^{2\ell+d-3}}{b_3^{\text{far}}}$ , given in Eq. (81) and in Eq. (85). This gives an expression for both real and imaginary part of  $\delta$ . There is more interest in the real part of  $\delta$  to give the estimation of the imaginary part of the QNM frequencies. Only considering the leading order of  $\frac{r_h}{l}$ , we have that the real part of

$\delta$  defined as  $\Re\epsilon\delta$  is

$$\Re\epsilon\delta = -\frac{2\Gamma[k + \ell + \frac{d-3}{2} + \gamma] \Gamma^2\left[1 + \frac{\ell+1}{d-3}\right]}{k! (2\ell + d - 3) \Gamma[\gamma + k]} \times \frac{\Gamma^2\left[1 + \frac{\ell-1}{d-3}\right] \left(\ell + \frac{d-1}{2}\right)_k \left(\frac{r_h}{l}\right)^{2\ell+d-2}}{\Gamma^2\left[1 + \frac{2\ell}{d-3}\right] \Gamma\left[\ell + \frac{d-3}{2}\right]} \omega_{\text{AdS}}, \quad (86)$$

where  $\gamma = 1 + \frac{1}{2}\sqrt{(d-3)^2 + 4\mu^2 l^2}$ . We note that  $\Re\epsilon\delta \sim (\frac{r_h}{l})^{2\ell+d-2}$ , which is the same result for scalar field perturbations in  $d$ -dimensional Reissner-Nordström-AdS black holes [47]. Also,  $\Re\epsilon\delta < 0$ , as expected from the linear stability analysis. We recall that Eq. (86) only holds for noninteger  $\frac{2\ell}{d-3}$ . This means that it does not formally hold for  $d = 4, 5$ , and neither for the specific values of  $\ell = \frac{m(d-3)}{2}$ ,  $m = 1, 2, \dots$  when  $d \geq 6$ .

The validity of Eq. (86) could be in principle tested by fitting the numerical results to  $\Re\epsilon\delta = -P(\frac{r_h}{l})^Q$ , with  $P, Q$  parameters, and comparing  $P, Q$  with the ones predicted by the analytical expression. As stated in the beginning of this section, the numerical results are not accurate enough for sufficiently small black holes. Typically, for  $\omega$  with  $|\Im(\omega l)| \lesssim 10^{-11}$ , the QNM frequencies obtained from numerically integrating the Schrödinger-like equations oscillate substantially when one changes the initial guess or the domain of integration. Since the magnitude of the imaginary part of the frequencies decreases as  $(\frac{r_h}{l})^{2\ell+d-2}$ , this means that the numerical results are only accurate for  $\frac{r_h}{l} \gtrsim 0.01$ . Thus, numerical verification of Eq. (86) is still needed, possibly using the Breit-Wigner resonance method approached in [21, 46]. Comparison between analytical and numerical results is done in Table V. The analytical and numerical results of Table V agree up to the second significant figure. A better agreement could in principle be achieved for smaller black holes, although for that to happen our numerical methods need to be improved.

	$k$	$\mu$	$\Re\epsilon\delta_{nl}$	$\Re\epsilon\delta_{al}$
$d = 6$	0	0	$-1.758 \times 10^{-9}$	$-1.738 \times 10^{-9}$
	0	0.5	$-1.906 \times 10^{-9}$	$-1.883 \times 10^{-9}$
	1	0.5	$-1.849 \times 10^{-8}$	$-1.809 \times 10^{-8}$
$d = 7$	0	0	$-7.725 \times 10^{-11}$	$-7.680 \times 10^{-11}$
	0	0.5	$-8.188 \times 10^{-11}$	$-8.139 \times 10^{-11}$
	1	0.5	$-8.665 \times 10^{-10}$	$-8.572 \times 10^{-10}$

TABLE V. Comparison between numerical results for the real part of  $\delta l$ ,  $\Re\epsilon\delta_{nl}$ , and analytical results obtained from Eq. (86),  $\Re\epsilon\delta_{al}$ , for different parameters of the vector-type  $\ell = 1$  Proca perturbation in  $d = 6, 7$  Schwarzschild-AdS black holes, with radius  $\frac{r_h}{l} = 0.02$ .

Interestingly, we have found that the numerical results obey Eq. (86) even for integer  $\frac{2\ell}{d-3}$ , which seems to indicate that the solutions can still be matched as if there was no logarithmic term. Such might be due to the approximations done in  $\omega r$  and  $\frac{r}{l}$ , in order to solve analytically

the Schödinger-like equation in the near region, although further investigation is still needed in this regard.

Note that the agreement between analytical and numerical results for monopole perturbations is much more satisfactory than for vector-type perturbations. Indeed, since the monopole frequencies decrease slowly with the radius of the black hole, we were able to obtain numerical results for smaller black holes, for which the approximations of the analytical method are better.

### C. Maxwell perturbations: Matched asymptotic expansions

#### 1. Scalar-type Maxwell perturbations

##### Near region

We now perform the matching asymptotic expansions for the Maxwell field in a Schwarzschild-AdS black hole background, a procedure that, to our knowledge, has not yet been carried out explicitly in  $d$  spacetime dimensions. While similar techniques have been extensively applied to scalar and gravitational fields, the analogous analysis for the Maxwell field remains unexplored in higher-dimensional settings. This analysis is crucial for understanding the asymptotic structure of electrodynamics in arbitrary dimensions and may provide insight into the behavior of electromagnetic radiation, conserved charges, and symmetry structures at null infinity.

We start by treating the scalar-type case of the Maxwell field. The scalar-type modes are described by Eqs. (19) and (20). By performing the transformation in Eq. (66), i.e.,  $z \equiv z(r) = 1 - \left(\frac{r_h}{r}\right)^{d-3}$ , the equation for these Maxwell modes in the near region becomes

$$\begin{aligned} & z(1-z) \frac{d^2 u_{12}^{\text{near}}}{dz^2} + \left(1 - z \left(2 + \frac{1}{d-3}\right)\right) \frac{du_{12}^{\text{near}}}{dz} \\ & + \frac{1}{(d-3)^2} \left( \frac{\omega^2 r_h^2}{z(1-z)} - \frac{l(l+d-3)}{1-z} \right. \\ & \left. - \frac{(d-2)(d-4)z}{4(1-z)} + \frac{(d-4)(d-3)}{2} \right) u_{12}^{\text{near}} = 0, \end{aligned} \quad (87)$$

where  $u_{12}^{\text{near}}$  is the solution  $u_{12}$  of the scalar-type modes in the near region. Equation (87) can be solved by a hypergeometric function, having thus  $u_{12}^{\text{near}} = cz^{-\frac{i\omega r_h}{d-3}} (1-z)^{\frac{2\ell+d-4}{2(d-3)}} {}_2F_1\left[\frac{\ell}{d-3} - i\bar{\omega}, 2 + \frac{\ell}{d-3} - i\bar{\omega}, 1 - 2i\bar{\omega}; z\right]$ , where  $c$  is a constant and  $\bar{\omega} = \frac{\omega r_h}{d-3}$ . Now, we must evaluate the solution asymptotically in the overlap region by studying the behaviour of the solution for  $z \rightarrow 1$ . One can do this by applying the transformation  $z \rightarrow 1 - z$  of the hypergeometric function. If  $\frac{2\ell}{d-3}$  is a non-integer, then

the solution in the overlap region is described by

$$\begin{aligned} u_{12}^{\text{near}} &= ca_{12}^{\text{near}} \left(\frac{r_h}{r}\right)^{\frac{2\ell+d-4}{2}} + cb_{12}^{\text{near}} \left(\frac{r}{r_h}\right)^{\frac{2\ell+d-2}{2}}, \\ a_{12}^{\text{near}} &= \frac{\Gamma[1 - 2i\bar{\omega}] \Gamma\left[-1 - \frac{2\ell}{d-3}\right]}{\Gamma\left[1 - \frac{\ell}{d-3} - i\bar{\omega}\right] \Gamma\left[-1 - \frac{\ell}{d-3} - i\bar{\omega}\right]}, \\ b_{12}^{\text{near}} &= \frac{\Gamma[1 - 2i\bar{\omega}] \Gamma\left[1 + \frac{2\ell}{d-3}\right]}{\Gamma\left[\frac{\ell}{d-3} - i\bar{\omega}\right] \Gamma\left[2 + \frac{\ell}{d-3} - i\bar{\omega}\right]}. \end{aligned} \quad (88)$$

To perform the matching, we must calculate the ratio between  $a_{12}^{\text{near}}$  and  $b_{12}^{\text{near}}$  for small  $\bar{\omega}$ . For a noninteger  $\frac{2\ell}{d-3}$ , we have

$$\begin{aligned} \frac{a_{12}^{\text{near}} r_h^{2\ell+d-3}}{b_{12}^{\text{near}}} &= \frac{(d-3)\Gamma^2\left[\frac{\ell}{d-3}\right]\Gamma^2\left[2 + \frac{\ell}{d-3}\right]r_h^{2\ell+d-3}}{(2\ell+d-3)\Gamma^2\left[1 + \frac{2\ell}{d-3}\right]} \\ &\times \left( \frac{\tan\left(\frac{\pi\ell}{d-3}\right)}{2\pi} + i\bar{\omega} \right), \end{aligned} \quad (89)$$

where the equality is approximate. For the case of  $\frac{2\ell}{d-3}$  being an integer, the solution evaluated in the overlap region has a logarithmic term which forbids the matching.

##### Far region

To analyze the scalar-type modes of the Maxwell field in the far region, we need to perform the transformation in Eq. (71), i.e.,  $y \equiv y(r) = \left(1 + \frac{r^2}{l^2}\right)^{-1}$ , to Eqs. (19) and (20), and only consider leading order terms in  $r_h$ , as we are in the approximation  $\frac{r-r_h}{l} \gg \frac{r_h}{l}$ . The equation for the field in this approximation becomes

$$\begin{aligned} & y(1-y) \frac{\partial^2 u_{12}^{\text{far}}}{\partial y^2} + \left(\frac{1}{2} - y\right) \frac{\partial u_{12}^{\text{far}}}{\partial y} \\ & + \left(\frac{\omega^2 l^2}{4} - \frac{\ell(\ell+d-3)}{4(1-y)} \right. \\ & \left. - \frac{(d-2)(d-4)}{16y(1-y)} + \frac{d-4}{4y}\right) u_{12}^{\text{far}} = 0. \end{aligned} \quad (90)$$

The solution to Eq. (90), in the far region, that obeys the Dirichlet boundary conditions at infinity is described by the hypergeometric function as  $u_{12}^{\text{far}} = y^{\frac{d-4}{4}} (1-y)^{\frac{2\ell+d-2}{4}} {}_2F_1\left[\frac{\ell+d-3+\omega l}{2}, \frac{\ell+d-3-\omega l}{2}; \frac{d-3}{2}; y\right]$  for  $d \geq 5$  and for  $d = 4$ , it is  $u_{12}^{\text{far}} = y^{\frac{1}{2}} (1-y)^{\frac{\ell+1}{2}} {}_2F_1\left[1 + \frac{\ell+\omega l}{2}, 1 + \frac{\ell-\omega l}{2}; \frac{3}{2}; y\right]$ . However, since for  $d = 4$ , the near region is not valid, we shall also omit the  $d = 4$  case from the analysis.

The solution in the far region can be evaluated at the overlap region, at  $y = 1$ , by performing the transformation  $y \rightarrow 1 - y$  in the hypergeometric function. For noninteger  $-\ell - \frac{d-3}{2}$  and for  $d \neq 4$ , the solution can be

expanded as

$$u_{12}^{\text{far}}(r) = ca_{12}^{\text{far}} \left(\frac{r}{l}\right)^{-\frac{2\ell+d-4}{2}} + cb_{12}^{\text{far}} \left(\frac{r}{l}\right)^{\frac{2\ell+d-2}{2}} \quad (91)$$

$$a_{12}^{\text{far}} = \frac{\Gamma[\ell + \frac{d-3}{2}]}{\Gamma[\frac{\ell+d-3+\omega l}{2}]\Gamma[\frac{\ell+d-3-\omega l}{2}]}, \quad (92)$$

$$b_{12}^{\text{far}} = \frac{\Gamma[-\ell - \frac{d-3}{2}]}{\Gamma[-\frac{\ell+\omega l}{2}]\Gamma[-\frac{\ell-\omega l}{2}]}, \quad (93)$$

where  $\omega l = \omega_{\text{AdS}}l + i\delta l$ , with  $\omega_{\text{AdS}}l = 2k + \ell + d - 3$ . Recall that this expression only describes the case  $d \geq 5$ . The ratio between the two coefficients for small  $\delta$  becomes

$$\frac{a_{12}^{\text{far}} l^{2\ell+d-3}}{b_{12}^{\text{far}}} = -\frac{k!\Gamma[\ell + \frac{d-3}{2}]\Gamma[k + \frac{d-3}{2}]l^{2\ell+d-2}}{2\Gamma[k + \ell + d - 3] \left(\ell + \frac{d-1}{2}\right)_k} i\delta. \quad (94)$$

### Overlap region

We can then connect the near region and the far region expressions in the overlap region. The matching condition is given by ensuring that the field and its first derivative are continuous, meaning that  $\frac{a_{12}^{\text{far}} l^{2\ell+d-3}}{b_{12}^{\text{far}}} = \frac{a_{12}^{\text{near}} r_1^{2\ell+d-3}}{b_{12}^{\text{near}}}$ . This gives an expression for the real and imaginary part of  $\delta$ . We shall only consider  $\Re\epsilon\delta$  since it describes the decay of the modes, and its expression is

$$\Re\epsilon\delta = -\frac{2\Gamma^2[\frac{\ell}{d-3}]\Gamma^2[2 + \frac{\ell}{d-3}]}{(2\ell + d - 3)\Gamma^2[1 + \frac{2\ell}{d-3}]\Gamma[\ell + \frac{d-3}{2}]} \times \frac{\Gamma[k + \ell + d - 3]}{k!\Gamma[k + \frac{d-3}{2}]} \left(\ell + \frac{d-1}{2}\right)_k \left(\frac{r_h}{l}\right)^{2\ell+d-2} \omega_{\text{AdS}}, \quad (95)$$

which is only valid for non-integer  $\frac{2\ell}{d-3}$  and non-integer  $-\ell - \frac{d-3}{2}$ . Again, one can observe that the decay goes as  $\Re\epsilon\delta \sim \left(\frac{r_h}{l}\right)^{2\ell+d-2}$ . We have compared the analytic results in Eq. (95) with the numerical results, which are summarized in Table VI. The values of the analytical expression match the numerical ones up to the second significant digit.

	$\ell$	$\Re\epsilon\delta_{n,l}$	$\Re\epsilon\delta_{a,l}$
$d = 6$	1	$-1.156 \times 10^{-4}$	$-1.017 \times 10^{-4}$
	4	$-1.153 \times 10^{-11}$	$-7.552 \times 10^{-12}$
$d = 8$	1	$-1.342 \times 10^{-5}$	$-1.513 \times 10^{-5}$

TABLE VI. Comparison between numerical results for the real part of  $\delta l$ ,  $\Re\epsilon\delta_{n,l}$ , and analytical results obtained from Eq. (95),  $\Re\epsilon\delta_{a,l}$ , for different parameters of the scalar-type  $k = 0$  electromagnetic Maxwell perturbation in  $d = 6, 8$  Schwarzschild-AdS black holes, with radius  $\frac{r_h}{l} = 0.01$ .

### 2. Vector-type Maxwell perturbations

Regarding the vector-type Maxwell perturbations, the QNM frequencies  $\omega = \omega_{\text{AdS}} + i\delta$  follow from the vector-

type Proca perturbations by setting  $\mu = 0$ . In particular, the real part of  $\delta$  for the vector-type electromagnetic perturbations is given by Eq. (86) with  $\mu = 0$ , and so  $\gamma = 1 + \frac{1}{2}\sqrt{(d-3)^2}$ , yielding

$$\Re\epsilon\delta = -\frac{2\Gamma[k + \ell + d - 2]\Gamma^2\left[1 + \frac{\ell+1}{d-3}\right]}{k!(2\ell + d - 3)\Gamma\left[\frac{d-1}{2} + k\right]} \times \frac{\Gamma^2\left[1 + \frac{\ell-1}{d-3}\right] \left(\ell + \frac{d-1}{2}\right)_k \left(\frac{r_h}{l}\right)^{2\ell+d-2}}{\Gamma^2\left[1 + \frac{2\ell}{d-3}\right] \Gamma\left[\ell + \frac{d-3}{2}\right]} \omega_{\text{AdS}}, \quad (96)$$

where  $\omega_{\text{AdS}} = 2k + \ell + d - 2$ . Note that, like the Proca case, this expression is only valid for non-integer  $\frac{2\ell}{d-3}$ . The comparison between the analytical expression and the numerical values are displayed in Table V when  $\mu = 0$ .

## VIII. CONCLUSIONS

We studied the QNMs of Proca and Maxwell field perturbations in  $d$ -dimensional Schwarzschild-AdS spacetimes with Dirichlet boundary conditions at infinity.

We reviewed how the Proca field equations in a static and spherically symmetric  $d$ -dimensional background reduce to a set of three radial wave-like equations: one equation describing the  $d - 3$  vector-type modes of the Proca field, which are completely decoupled, and two coupled equations describing the two scalar-type modes of the Proca field. Unlike in pure AdS, in Schwarzschild-AdS the scalar-type modes are nontrivially coupled, which makes their analysis substantially more involved. We also showed how the Maxwell field equations, as a zero mass limit of the Proca equations, can be obtained. The two coupled Proca degrees of freedom were distinguished in the massless limit, where there is a pure gauge degree of freedom that obeys the Klein-Gordon equation, and a Maxwell physical degree of freedom that obeys the scalar-type Maxwell equation. With such distinction made, we inferred by back propagation which of the two coupled Proca modes gives the gauge and physical modes in the massless limit. The Proca nonelectromagnetic polarization mode was shown to give the Maxwell gauge mode, whereas the Proca electromagnetic polarization mode was shown to give the Maxwell physical mode. In  $d = 4$ , however, the scalar-type Maxwell mode does not follow smoothly from the massless limit of the Proca mode with electromagnetic polarization. Such happens due to the vanishing of the effective mass,  $\mu_{\text{eff}}^2 = \mu^2 + \frac{(d-2)(d-4)}{4l^2}$ , which changes the behavior of the potential at infinity. In this case, the Maxwell scalar-type modes obey exactly the same equation as the vector-type modes, and the Maxwell modes can be obtained smoothly from the massless limit of the vector-type Proca modes.

The QNMs of these fields were obtained numerically for 4, 5, 6, 7-dimensional Schwarzschild-AdS black holes. Generalization to other higher dimensions should be

straightforward. For all the dimensions  $d$  and all the perturbation types, both real and imaginary parts of the frequencies increased with increasing mass of the Proca field, in agreement with previous works for  $d = 4$ . Proca field perturbations were found to show no isospectrality. On the other hand Maxwell perturbations of scalar-type and vector-type were found to be isospectral in the large black hole regime, for all the spacetime dimensions. Such isospectrality was proved analytically, using the mathematical machinery developed by Chandrasekhar. Taking into consideration Proca perturbations, our numerical results suggest that the isospectrality is preserved between Maxwell scalar-type and vector-type modes with electromagnetic polarization.

The effect of the black hole radius on the Proca QNM frequencies was also investigated. For large black holes, with  $r_h \gg l$ , most Proca mode frequencies scale linearly with the black hole radius, in accordance with previous works. Scalar-type Maxwell perturbations in  $d \geq 5$  large Schwarzschild-AdS black holes also exhibit purely imaginary low frequency modes, whose expression was found analytically to scale with the inverse of the black hole radius and with the square of the angular momentum number of the perturbation. The numerical results showed good support for the analytical expression. Such low frequency modes were found in previous studies for vector-type gravitational perturbations, and have a clear meaning within the AdS/CFT correspondence, being associated to the hydrodynamic modes of the dual field theory. It would be interesting to check if the results from the CFT side match ours. When the radius of the black hole is of the same order as the radius of AdS,  $r_h \simeq l$ , the linear behavior breaks down, with the real part of the frequencies approaching a minimum, which may be due to the black hole starting to have a comparable size with the Compton wavelength of the field. In the limit of vanishing radius, the frequencies approach those of pure AdS. Namely, scalar-type Proca frequencies with electromagnetic and nonelectromagnetic polarizations approach, respectively, the scalar-type Proca frequencies of pure AdS with total angular momentum number  $j = \ell - 1$  and  $j = \ell + 1$ . Similarly, vector-type Proca frequencies approach the vector-type  $j = \ell$  frequencies of pure AdS. When the radius of the black hole is much less than the radius of AdS,  $r_h \ll l$ , one is in the small black hole regime. Numerical methods do not yield reliable results in this regime. However, we were able to obtain analytical expressions for the frequencies' imaginary part,  $\delta$ , of vector-type and monopole Proca perturbations, and also Maxwell perturbations, in the small black hole regime. This was done by matching asymptotic expansions of the solution in an overlap region, which forms if the Compton wavelength of the Proca particle is much larger than the radius of the black hole. For vector-type perturbations the imaginary part scales as  $\delta \sim (\frac{r_h}{l})^{2\ell+d-2} \omega_{\text{AdS}}$ , whereas for monopole perturbations it scales as  $\delta \sim (\frac{r_h}{l})^{d-2} \omega_{\text{AdS}}^{-1}$ , where  $\omega_{\text{AdS}}$  is the corresponding pure AdS normal mode frequency. The

numerical results show support for the analytical expressions, although it would be interesting to implement more suitable numerical methods to verify our analytical predictions.

## ACKNOWLEDGMENTS

The authors thank the financial support from Fundação para a Ciência e Tecnologia - FCT through the project No. UIDB/00099/2025 and project No. UIDP/00099/2025, namely T. F. thanks for the financial support through the grant FCT no. RD 1415.

## Appendix A: Horowitz-Hubeny method for computation of quasinormal modes in Schwarzschild-AdS

### 1. Preamble

In Sec. V we introduced our own numerical method based on the shooting method, and mentioned that we have also used, as way of comparing the results, the Horowitz-Hubeny method [31]. We now present the Horowitz-Hubeny method. This method is widely used to compute QNMs in asymptotically AdS spacetimes, using the fact that the eigenvalue problem involves an equation with regular singular points together with the Dirichlet boundary condition.

### 2. Horowitz-Hubeny numerical integration method for the Proca field: Decoupled and coupled Schrödinger-like equations

#### a. Scalar-type $\ell = 0$ monopole Proca field and vector-type Proca field: Decoupled Schrödinger-like equation

The Horowitz-Hubeny method in the Proca field case can be applied to the monopole case of the scalar-type Proca field described by  $u_1$  with  $u_2 = 0$ , since in this case, the coupled system of equations reduces to a single equation. It can also be applied to the vector-type Proca field. We explain the method applied to the vector-type Proca field, the other cases follow with ease.

The vector-type sector of the Proca field is described by a single Schrödinger-like equation in Eq. (16). It is useful to rewrite the vector-type radial function  $u_3(r)$  as  $u_3(r) = e^{-i\omega r_*} \psi_3(r)$ , where  $\psi_3(r)$  obeys now

$$\partial_r^2 \psi_3 + \frac{(f' - 2i\omega)}{f} \partial_r \psi_3 - \frac{V_v}{f^2} \psi_3 = 0. \quad (\text{A1})$$

The equation has formally  $d + 1$  regular singular points, with the zeroes of  $f$  corresponding to  $d - 1$  regular singular points, with  $r = r_h$  being one of them, together with the points  $r = 0$  and  $r = +\infty$ . The  $r = +\infty$  singularity

is studied by writing  $x = \frac{1}{r}$ , with range  $x \in (0, \frac{1}{r_h}]$ , which is always finite in the range of interest. By doing such transformation, Eq. (A1) becomes

$$s(x)(x - x_h)\partial_x^2\psi_3 + t(x)\partial_x\psi_3 + \frac{v(x)}{(x - x_h)}\psi_3 = 0, \quad (\text{A2})$$

where

$$\begin{aligned} s(x) &= \frac{x^4 f}{x - x_h}, \\ t(x) &= x^2 \partial_x (x^2 f) + 2i\omega x^2, \\ v(x) &= -\frac{(x - x_h) V_v(x)}{f}, \end{aligned} \quad (\text{A3})$$

with  $f$  and  $V_v$  written in terms of  $x$ . The Fuchs' theorem guarantees that Eq. (A2) admits a Frobenius solution near each of its regular singular points, namely, near  $x_h$ . The radius of convergence of the solution will be given by the minimum distance between  $x = x_h$  and the other  $d$  singular points in the complex plane. The expansion near the horizon  $x = x_h$  is described by

$$\psi_3(x) = (x - x_h)^\alpha \sum_{m=0}^{\infty} a_{(3)m}(x - x_h)^m, \quad (\text{A4})$$

where the exponent  $\alpha$  is a constant determined from the indicial equation after imposing the boundary condition at the horizon, and  $a_{(3)m}$  are coefficients that usually depend on the frequency i.e.,  $a_{(3)m} \equiv a_{(3)m}(\omega)$ , with  $a_{(3)m} \neq 0$ . The polynomials  $s(x)$ ,  $t(x)$ , and  $u(x)$  can also be expanded near the horizon, i.e.,  $s(x) = \sum_{p=0}^{\infty} s_p (x - x_h)^p$ ,  $t(x) = \sum_{p=0}^{\infty} t_p (x - x_h)^p$ , and  $v(x) = \sum_{p=0}^{\infty} v_p (x - x_h)^p$ , where  $s_p$ ,  $t_p$ , and  $v_p$  are coefficients independent of  $x$ . Substituting Eq. (A4) and the expanded polynomials  $s(x)$ ,  $t(x)$ , and  $v(x)$  in Eq. (A2), one gets

$$\begin{aligned} \sum_{m,p=0}^{\infty} [s_p(m + \alpha)(m + \alpha - 1) + t_p(m + \alpha) + v_p] \\ \times a_{(3)m} (x - x_h)^{m+\alpha+p} = 0. \end{aligned} \quad (\text{A5})$$

The term with  $m = p = 0$  gives rise to the indicial equation for  $\alpha$

$$s_0\alpha(\alpha - 1) + t_0\alpha + v_0 = 0. \quad (\text{A6})$$

Taking into account that  $s_0 = -x_h^2 f'(r_h)$ ,  $t_0 = 2x_h^2 \left(i\omega - \frac{f'(r_h)}{2}\right)$  and  $v_0 = 0$ , the solutions to Eq. (A6) are  $\alpha = 0$  or  $\alpha = \frac{2i\omega}{f'(r_h)}$ , corresponding, respectively, to ingoing and outgoing modes at the horizon. The boundary condition Eq. (28) or Eq. (30) sets  $\alpha = 0$ , so that only ingoing modes are allowed near the horizon. Setting this in Eq. (A5), relabelling indexes and equating the terms for each power of  $(x - x_h)$ , one arrives at the recursion

relation for the coefficients  $a_{(3)j}$ ,

$$\begin{aligned} a_{(3)j} &= -\frac{1}{P_j} \\ &\times \sum_{m=0}^{j-1} [m(m-1)s_{j-m} + mt_{j-m} + v_{j-m}] a_{(3)m}, \end{aligned} \quad (\text{A7})$$

where  $P_j = j(j-1)s_0 + jt_0$ . Without loss of generality, one can set  $a_{(3)0} = 1$  and solve recursively Eq. (A7) up to a given order,  $N$ . The Dirichlet boundary condition at spatial infinity then yields

$$\psi_3(x=0) = \sum_{m=0}^{\infty} a_{(3)m}(\omega) (-x_h)^m = 0, \quad (\text{A8})$$

which can be solved numerically for  $\omega$  by truncating the sum at a sufficiently large  $N$ . To see whether the  $N$  chosen is sufficiently large, one simply checks if the solution of the  $N$ -term sum is sufficiently close to the solution of the  $(N+1)$ -term sum, within the desired accuracy.

This method is also used in the monopole case of the scalar-type Proca field described by  $u_1$  with  $u_2 = 0$ , since in this case, the coupled system of equations reduces to a single equation. Indeed, one can follow the method explained with the replacement of the potential  $V_{s11}$  for the monopole scalar-type Proca field.

#### b. Scalar-type $\ell \geq 1$ Proca field: Coupled equations

Scalar-type Proca field perturbations are described by the coupled system Eq. (13), so that the Horowitz-Hubeny technique from the previous section needs to be slightly modified, as in [21, 50]. We define the vector  $\mathbf{u}(r) = (u_1, u_2)^T$  and make the transformation  $\mathbf{u}(r) = e^{-i\omega r_*} \boldsymbol{\psi}(r)$  in the coupled system, so that Eq. (13) can be written as

$$s(x)(x - x_h)\partial_x^2\boldsymbol{\psi} + t(x)\partial_x\boldsymbol{\psi} + \frac{\mathbf{v}(x)}{(x - x_h)}\boldsymbol{\psi} = 0, \quad (\text{A9})$$

with  $\mathbf{v}(x) = -\frac{(x-x_h)\mathbf{V}_s}{f}$ . After expanding  $\boldsymbol{\psi}(x)$  near the horizon as

$$\boldsymbol{\psi}(x) = \sum_{m=0}^{\infty} \mathbf{a}_j(\omega)(x - x_h)^j, \quad (\text{A10})$$

where  $\mathbf{a}_j$  are coefficients of the series and they are vectors, as well as expanding  $s(x)$  with coefficients  $s_j$ ,  $t(x)$  with coefficients  $t_j$  and  $\mathbf{v}(x)$  with coefficients  $\mathbf{v}_j$ , one obtains a recurrence relation for the coefficients  $\mathbf{a}_j$ , which can be related to the coefficient  $\mathbf{a}_0$  as  $\mathbf{a}_j(\omega) = \mathbf{B}_j(\omega)\mathbf{a}_0$  with matrices  $\mathbf{B}_j$  determined by

$$\begin{aligned} \mathbf{B}_j &= -\frac{1}{P_j} \\ &\times \sum_{m=0}^{j-1} [(m(m-1)s_{j-m} + mt_{j-m})\mathbf{I} + \mathbf{v}_{j-m}] \mathbf{B}_m, \end{aligned} \quad (\text{A11})$$

The Dirichlet boundary condition at spatial infinity then yields  $\psi(x=0) = \left(\sum_{j=0}^{\infty} \mathbf{B}_j(\omega)(-x_h)^j\right) \mathbf{a}_0 = 0$ , whose nontrivial solution fixes the values of  $\omega$  through

$$\det \left( \sum_{j=0}^{\infty} \mathbf{B}_j(\omega)(-x_h)^j \right) = 0. \quad (\text{A12})$$

As in the decoupled case, Eq. (A12) can be solved numerically for  $\omega$  by truncating the sum at a sufficiently large  $N$ .

### 3. Horowitz-Hubeny numerical integration method for the Maxwell field: Decoupled equations

The Maxwell field also yields decoupled equations. So under Dirichlet boundary condition, the method for decoupled Proca equations given above can in principle be applied.

The Horowitz-Hubeny numerical integration method can be applied to the scalar-type Maxwell field  $u_{12}$ . In-

stead, one can follow the same method as explained above with the replacement of the potential  $V_v$  by the potential  $V_s$  for the scalar-type Maxwell field. However, it cannot be applied to the specific case of the scalar-type Maxwell field in  $d=5$  since Dirichlet-Neumann boundary conditions are imposed and not Dirichlet.

The Horowitz-Hubeny numerical integration method can also be applied to the vector-type Maxwell field  $u_3$  with  $\mu=0$ . One can also follow the same method with the replacement of the potential  $V_v$  by the potential  $V_v$  with  $\mu=0$  for the vector-type Maxwell field.

### Appendix B: Numerical values for the Proca quasinormal modes

We present the numerical values in Tabs. I-IV of this Appendix, of the Proca QNMs in four, five, six and seven dimensions, for values of the black hole horizon  $r_h \in [0.05, 1, 100]$  and for values of the Proca mass  $\mu \in [0.1, 0.2, 0.3, 0.4, 0.5]$ , for the scalar-type and vector-type modes, and their polarizations, see also Sec. VI. We also include the electromagnetic limit for the electromagnetic polarized scalar-type and vector-type modes.

$r_h$	$\mu$	$\omega (d=4)$	$\omega (d=5)$	$\omega (d=6)$	$\omega (d=7)$
100	0.1	185.569 – 267.526 <i>i</i>	312.426 – 275.165 <i>i</i>	413.971 – 269.616 <i>i</i>	501.060 – 261.424 <i>i</i>
	0.2	187.346 – 270.819 <i>i</i>	313.801 – 276.650 <i>i</i>	415.038 – 270.457 <i>i</i>	501.916 – 261.962 <i>i</i>
	0.3	190.106 – 275.942 <i>i</i>	316.047 – 279.075 <i>i</i>	416.800 – 271.846 <i>i</i>	503.334 – 262.853 <i>i</i>
	0.4	193.636 – 282.504 <i>i</i>	319.103 – 282.376 <i>i</i>	419.234 – 273.765 <i>i</i>	505.304 – 264.092 <i>i</i>
	0.5	197.742 – 290.148 <i>i</i>	322.892 – 286.471 <i>i</i>	422.310 – 276.190 <i>i</i>	507.811 – 265.669 <i>i</i>
1	0.1	2.80724 – 2.68313 <i>i</i>	4.58507 – 2.55966 <i>i</i>	6.01308 – 2.35363 <i>i</i>	7.27221 – 2.16280 <i>i</i>
	0.2	2.83328 – 2.71753 <i>i</i>	4.60375 – 2.57442 <i>i</i>	6.02701 – 2.36168 <i>i</i>	7.28309 – 2.16779 <i>i</i>
	0.3	2.87379 – 2.77101 <i>i</i>	4.63430 – 2.59855 <i>i</i>	6.05003 – 2.37497 <i>i</i>	7.30115 – 2.17606 <i>i</i>
	0.4	2.92572 – 2.83946 <i>i</i>	4.67589 – 2.63137 <i>i</i>	6.08184 – 2.39332 <i>i</i>	7.32625 – 2.18756 <i>i</i>
	0.5	2.98623 – 2.91912 <i>i</i>	4.72755 – 2.67209 <i>i</i>	6.12207 – 2.41652 <i>i</i>	7.35822 – 2.20219 <i>i</i>
0.05	0.1	2.86292 – 1.94677 × 10 <sup>-2</sup> <i>i</i>	3.98937 – 1.75825 × 10 <sup>-3</sup> <i>i</i>	5.00162 – 1.81866 × 10 <sup>-4</sup> <i>i</i>	6.00231 – 1.94173 × 10 <sup>-5</sup> <i>i</i>
	0.2	2.88910 – 1.98707 × 10 <sup>-2</sup> <i>i</i>	4.00405 – 1.77507 × 10 <sup>-3</sup> <i>i</i>	5.01155 – 1.83002 × 10 <sup>-4</sup> <i>i</i>	6.00979 – 1.95086 × 10 <sup>-5</sup> <i>i</i>
	0.3	2.92988 – 2.05020 × 10 <sup>-2</sup> <i>i</i>	4.02805 – 1.80268 × 10 <sup>-3</sup> <i>i</i>	5.02797 – 1.84886 × 10 <sup>-4</sup> <i>i</i>	6.02219 – 1.96605 × 10 <sup>-5</sup> <i>i</i>
	0.4	2.98222 – 2.13182 × 10 <sup>-2</sup> <i>i</i>	4.06075 – 1.84049 × 10 <sup>-3</sup> <i>i</i>	5.05066 – 1.87503 × 10 <sup>-4</sup> <i>i</i>	6.03942 – 1.98727 × 10 <sup>-5</sup> <i>i</i>
	0.5	3.04330 – 2.22800 × 10 <sup>-2</sup> <i>i</i>	4.10136 – 1.88781 × 10 <sup>-3</sup> <i>i</i>	5.07935 – 1.90836 × 10 <sup>-4</sup> <i>i</i>	6.06136 – 2.01447 × 10 <sup>-5</sup> <i>i</i>

TABLE I. Fundamental modes of  $\ell=0$  Proca monopole scalar perturbations in 4, 5, 6, 7-dimensional Schwarzschild-AdS spacetime with  $r_h=100$ ,  $r_h=1$  and  $r_h=0.05$ , for different values of the mass of the field.

$r_h$	$\mu$	$\omega (d = 4)$	$\omega (d = 5)$	$\omega (d = 6)$	$\omega (d = 7)$
100	0.1	185.577 - 267.524 <i>i</i>	312.433 - 275.163 <i>i</i>	413.978 - 269.614 <i>i</i>	501.067 - 261.422 <i>i</i>
	0.2	187.354 - 270.817 <i>i</i>	313.808 - 276.648 <i>i</i>	415.045 - 270.455 <i>i</i>	501.922 - 261.960 <i>i</i>
	0.3	190.114 - 275.939 <i>i</i>	316.054 - 279.073 <i>i</i>	416.807 - 271.844 <i>i</i>	503.340 - 262.852 <i>i</i>
	0.4	193.644 - 282.501 <i>i</i>	319.110 - 282.374 <i>i</i>	419.241 - 273.763 <i>i</i>	505.310 - 264.090 <i>i</i>
	0.5	197.750 - 290.146 <i>i</i>	322.899 - 286.469 <i>i</i>	422.316 - 276.188 <i>i</i>	507.817 - 265.667 <i>i</i>
1	0.1	3.33865 - 2.50108 <i>i</i>	5.09680 - 2.38187 <i>i</i>	6.53418 - 2.18970 <i>i</i>	7.80878 - 2.01206 <i>i</i>
	0.2	3.36178 - 2.53440 <i>i</i>	5.11406 - 2.39630 <i>i</i>	6.54725 - 2.19759 <i>i</i>	7.81908 - 2.01696 <i>i</i>
	0.3	3.39782 - 2.58616 <i>i</i>	5.14229 - 2.41988 <i>i</i>	6.56884 - 2.21062 <i>i</i>	7.83617 - 2.02509 <i>i</i>
	0.4	3.44410 - 2.65233 <i>i</i>	5.18076 - 2.45195 <i>i</i>	6.59870 - 2.22862 <i>i</i>	7.85993 - 2.03638 <i>i</i>
	0.5	3.49817 - 2.72926 <i>i</i>	5.22860 - 2.49174 <i>i</i>	6.63649 - 2.25137 <i>i</i>	7.89019 - 2.05076 <i>i</i>
0.05	0.1	3.91824 - 4.75561 $\times 10^{-5}$ <i>i</i>	4.99732 - 7.18144 $\times 10^{-6}$ <i>i</i>	6.00264 - 8.72484 $\times 10^{-7}$ <i>i</i>	7.00244 - 9.88835 $\times 10^{-8}$ <i>i</i>
	0.2	3.94538 - 4.89806 $\times 10^{-5}$ <i>i</i>	5.01207 - 7.27222 $\times 10^{-6}$ <i>i</i>	6.01258 - 8.79410 $\times 10^{-7}$ <i>i</i>	7.00991 - 9.94624 $\times 10^{-8}$ <i>i</i>
	0.3	3.98765 - 5.12361 $\times 10^{-5}$ <i>i</i>	5.03619 - 7.42189 $\times 10^{-6}$ <i>i</i>	6.02901 - 8.90921 $\times 10^{-7}$ <i>i</i>	7.02231 - 1.00415 $\times 10^{-7}$ <i>i</i>
	0.4	4.04191 - 5.41980 $\times 10^{-5}$ <i>i</i>	5.06904 - 7.62824 $\times 10^{-6}$ <i>i</i>	6.05171 - 9.06995 $\times 10^{-7}$ <i>i</i>	7.03954 - 1.01750 $\times 10^{-7}$ <i>i</i>
	0.5	4.10524 - 5.77538 $\times 10^{-5}$ <i>i</i>	5.10986 - 7.88857 $\times 10^{-6}$ <i>i</i>	6.08042 - 9.27537 $\times 10^{-7}$ <i>i</i>	7.06149 - 1.03470 $\times 10^{-7}$ <i>i</i>

TABLE II. Fundamental modes of  $\ell = 1$  nonelectromagnetic polarized scalar-type Proca perturbations in 4, 5, 6, 7-dimensional Schwarzschild-AdS spacetime with  $r_h = 100$ ,  $r_h = 1$  and  $r_h = 0.05$ , for different values of the mass of the field.

$r_h$	$\mu$	$\omega (d = 4)$	$\omega (d = 5)$	$\omega (d = 6)$	$\omega (d = 7)$
100	0	0. - 150.048 <i>i</i>	200.013 - 200.003 <i>i</i>	299.447 - 200.490 <i>i</i>	383.681 - 199.896 <i>i</i>
	0.1	0. - 152.097 <i>i</i>	200.509 - 200.499 <i>i</i>	299.812 - 200.768 <i>i</i>	383.969 - 200.073 <i>i</i>
	0.2	0. - 158.412 <i>i</i>	201.990 - 201.980 <i>i</i>	300.902 - 201.599 <i>i</i>	384.830 - 200.604 <i>i</i>
	0.3	0. - 168.740 <i>i</i>	204.413 - 204.403 <i>i</i>	302.704 - 202.972 <i>i</i>	386.257 - 201.485 <i>i</i>
	0.4	0. - 183.124 <i>i</i>	207.714 - 207.703 <i>i</i>	305.194 - 204.871 <i>i</i>	388.242 - 202.709 <i>i</i>
	0.5	0. - 202.409 <i>i</i>	211.814 - 211.803 <i>i</i>	308.345 - 207.272 <i>i</i>	390.770 - 204.269 <i>i</i>
1	0	2.16302 - 1.69909 <i>i</i>	2.66237 - 1.58299 <i>i</i>	4.41406 - 1.68956 <i>i</i>	5.73731 - 1.59713 <i>i</i>
	0.1	1.55730 - 0.552855 <i>i</i>	2.66878 - 1.59009 <i>i</i>	4.41877 - 1.69234 <i>i</i>	5.74090 - 1.59879 <i>i</i>
	0.2	1.56806 - 0.584611 <i>i</i>	2.68791 - 1.61115 <i>i</i>	4.43286 - 1.70062 <i>i</i>	5.75162 - 1.60373 <i>i</i>
	0.3	1.58497 - 0.634989 <i>i</i>	2.71949 - 1.64544 <i>i</i>	4.45614 - 1.71432 <i>i</i>	5.76942 - 1.61194 <i>i</i>
	0.4	1.60693 - 0.700879 <i>i</i>	2.76308 - 1.69187 <i>i</i>	4.48836 - 1.73324 <i>i</i>	5.79417 - 1.62335 <i>i</i>
	0.5	1.63296 - 0.779477 <i>i</i>	2.81810 - 1.74904 <i>i</i>	4.52915 - 1.75717 <i>i</i>	5.82571 - 1.63789 <i>i</i>
0.05	0	2.93223 - 5.39171 $\times 10^{-5}$ <i>i</i>	2.99617 - 5.74443 $\times 10^{-6}$ <i>i</i>	3.99948 - 1.65071 $\times 10^{-6}$ <i>i</i>	4.99994 - 3.35996 $\times 10^{-7}$ <i>i</i>
	0.1	1.98737 - 7.62153 $\times 10^{-6}$ <i>i</i>	3.00114 - 5.79865 $\times 10^{-6}$ <i>i</i>	4.00281 - 1.65889 $\times 10^{-6}$ <i>i</i>	5.00243 - 3.37073 $\times 10^{-7}$ <i>i</i>
	0.2	2.01476 - 8.30304 $\times 10^{-6}$ <i>i</i>	3.01589 - 5.96200 $\times 10^{-6}$ <i>i</i>	4.01275 - 1.68350 $\times 10^{-6}$ <i>i</i>	5.00991 - 3.40313 $\times 10^{-7}$ <i>i</i>
	0.3	2.05739 - 9.44648 $\times 10^{-6}$ <i>i</i>	3.04000 - 6.23648 $\times 10^{-6}$ <i>i</i>	4.02917 - 1.72478 $\times 10^{-6}$ <i>i</i>	5.02231 - 3.45740 $\times 10^{-7}$ <i>i</i>
	0.4	2.11204 - 1.10687 $\times 10^{-5}$ <i>i</i>	3.07285 - 6.62545 $\times 10^{-6}$ <i>i</i>	4.05187 - 1.78312 $\times 10^{-6}$ <i>i</i>	5.03954 - 3.53396 $\times 10^{-7}$ <i>i</i>
	0.5	2.17574 - 1.31994 $\times 10^{-5}$ <i>i</i>	3.11366 - 7.13369 $\times 10^{-6}$ <i>i</i>	4.08058 - 1.85907 $\times 10^{-6}$ <i>i</i>	5.06149 - 3.63339 $\times 10^{-7}$ <i>i</i>

TABLE III. Fundamental modes of  $\ell = 1$  electromagnetically polarized scalar-type Proca perturbations and the scalar-type Maxwell modes in 4, 5, 6, 7-dimensional Schwarzschild-AdS spacetime with  $r_h = 100$ ,  $r_h = 1$  and  $r_h = 0.05$ , for different values of the mass for the case of the Proca field. The case  $\mu = 0$  denotes the Maxwell mode and not the massless limit for  $d = 4$ .

$r_h$	$\mu$	$\omega (d = 4)$	$\omega (d = 5)$	$\omega (d = 6)$	$\omega (d = 7)$
100	0	0. - 150.048 <i>i</i>	200.026 - 199.995 <i>i</i>	299.458 - 200.486 <i>i</i>	383.691 - 199.894 <i>i</i>
	0.1	0. - 152.185 <i>i</i>	200.525 - 200.493 <i>i</i>	299.823 - 200.765 <i>i</i>	383.979 - 200.071 <i>i</i>
	0.2	0. - 158.505 <i>i</i>	202.007 - 201.975 <i>i</i>	300.914 - 201.596 <i>i</i>	384.839 - 200.602 <i>i</i>
	0.3	0. - 168.844 <i>i</i>	204.429 - 204.398 <i>i</i>	302.715 - 202.969 <i>i</i>	386.267 - 201.483 <i>i</i>
	0.4	0. - 183.251 <i>i</i>	207.729 - 207.698 <i>i</i>	305.205 - 204.868 <i>i</i>	388.252 - 202.707 <i>i</i>
	0.5	0. - 202.583 <i>i</i>	211.829 - 211.798 <i>i</i>	308.356 - 207.269 <i>i</i>	390.780 - 204.266 <i>i</i>
1	0	2.16302 - 1.69909 <i>i</i>	3.84177 - 1.62618 <i>i</i>	5.20392 - 1.53559 <i>i</i>	6.43969 - 1.45072 <i>i</i>
	0.1	2.17058 - 1.71095 <i>i</i>	3.84730 - 1.63091 <i>i</i>	5.20810 - 1.53813 <i>i</i>	6.44299 - 1.45229 <i>i</i>
	0.2	2.19254 - 1.74526 <i>i</i>	3.86377 - 1.64499 <i>i</i>	5.22058 - 1.54573 <i>i</i>	6.45286 - 1.45699 <i>i</i>
	0.3	2.22707 - 1.79879 <i>i</i>	3.89075 - 1.66805 <i>i</i>	5.24123 - 1.55828 <i>i</i>	6.46923 - 1.46480 <i>i</i>
	0.4	2.27191 - 1.86765 <i>i</i>	3.92761 - 1.69952 <i>i</i>	5.26981 - 1.57567 <i>i</i>	6.49202 - 1.47565 <i>i</i>
	0.5	2.32497 - 1.94823 <i>i</i>	3.97359 - 1.73872 <i>i</i>	5.30603 - 1.59769 <i>i</i>	6.52107 - 1.48949 <i>i</i>
0.05	0	2.93223 - 5.39171 $\times 10^{-5}i$	3.99493 - 4.36325 $\times 10^{-6}i$	4.99957 - 4.53425 $\times 10^{-7}i$	5.99996 - 4.85953 $\times 10^{-8}i$
	0.1	2.94163 - 5.46847 $\times 10^{-5}i$	3.99999 - 4.38818 $\times 10^{-6}i$	5.00290 - 4.54977 $\times 10^{-7}i$	6.00246 - 4.87122 $\times 10^{-8}i$
	0.2	2.96881 - 5.69458 $\times 10^{-5}i$	4.01466 - 4.46281 $\times 10^{-6}i$	5.01284 - 4.59635 $\times 10^{-7}i$	6.00994 - 4.90633 $\times 10^{-8}i$
	0.3	3.01112 - 6.05978 $\times 10^{-5}i$	4.03879 - 4.58669 $\times 10^{-6}i$	5.02927 - 4.67405 $\times 10^{-7}i$	6.02234 - 4.96497 $\times 10^{-8}i$
	0.4	3.06541 - 6.55234 $\times 10^{-5}i$	4.07167 - 4.75922 $\times 10^{-6}i$	5.05197 - 4.78298 $\times 10^{-7}i$	6.03957 - 5.04733 $\times 10^{-8}i$
	0.5	3.12875 - 7.16258 $\times 10^{-5}i$	4.11251 - 4.97971 $\times 10^{-6}i$	5.08069 - 4.92331 $\times 10^{-7}i$	6.06151 - 5.15367 $\times 10^{-8}i$

TABLE IV. Fundamental modes of  $\ell = 1$  vector-type Proca perturbations in 4, 5, 6, 7-dimensional Schwarzschild-AdS spacetime with  $r_h = 100$ ,  $r_h = 1$  and  $r_h = 0.05$ , for different values of the mass for the case of the Proca field. The case  $\mu = 0$  is the fundamental modes of  $\ell = 1$  vector-type Maxwell field.

- 
- [1] T. Regge and J. A. Wheeler, “Stability of a Schwarzschild singularity”, *Phys. Rev.* **108**, 1063 (1957).
- [2] F. J. Zerilli, “Effective potential for even-parity Regge-Wheeler gravitational perturbation equations”, *Phys. Rev. Lett.* **24**, 737 (1970).
- [3] C. V. Vishveshwara, “Stability of the Schwarzschild Metric”, *Phys. Rev. D* **1**, 2870 (1970).
- [4] R. Ruffini, J. Tiomno, and C. V. Vishveshwara, “Electromagnetic field of a particle moving in a spherically symmetric black hole background”, *Lett. Nuovo Cimento* **3**, 211 (1972).
- [5] S. A. Teukolsky, “Rotating black holes: Separable wave equations for gravitational and electromagnetic perturbations”, *Phys. Rev. Lett.* **20**, 1114 (1972).
- [6] S. Chandrasekhar and S. Detweiler, “The quasinormal modes of the Schwarzschild black hole”, *Proc. R. Soc. A* **344**, 441 (1975).
- [7] S. Chandrasekhar, *The Mathematical Theory of Black Holes* (Oxford University Press, New York, 1983).
- [8] D. V. Gal’tsov, G. V. Pomerantseva, and G. A. Chizhov, “Behavior of massive vector particles in a Schwarzschild field”, *Sov. Phys. J.* **27**, 697 (1984).
- [9] L. E. Simone and C. M. Will, “Massive scalar quasinormal modes of Schwarzschild and Kerr black holes”, *Classical Quantum Gravity* **9**, 963 (1992).
- [10] K. D. Kokkotas and B. G. Schmidt, “Quasinormal modes of stars and black holes”, *Living Rev. Rel* **2** (1999) 2; arXiv:gr-qc/9909058 [gr-qc].
- [11] L. C. B. Crispino, A. Higuchi, and G. E. A. Matsas, “Quantization of the electromagnetic field outside static black holes and its application to low-energy phenomena”, *Phys. Rev. D* **63**, 124008 (2001); arXiv:gr-qc/0011070.
- [12] A. Pawl, “The timescale for loss of massive vector hair by a black hole and its consequences for proton decay”, *Phys. Rev. D* **70**, 124005 (2004); arXiv:hep-th/0411175.
- [13] R. A. Konoplya and A. V. Zhidenko, “Decay of massive scalar field in a Schwarzschild background”, *Phys. Lett. B* **609**, 377 (2005); arXiv:gr-qc/0411059.
- [14] A. V. Zhidenko, “Massive scalar field quasinormal modes of higher dimensional black holes”, *Phys. Rev. D* **74**, 064017 (2006); arXiv:gr-qc/0607133.
- [15] V. Cardoso, O. J. C. Dias, J. P. S. Lemos, S. Yoshida, “The black hole bomb and superradiant instabilities”, *Phys. Rev. D* **70**, 044039 (2004); arXiv:hep-th/0404096.
- [16] R. A. Konoplya, “Massive vector field perturbations in the Schwarzschild background: Stability and quasinormal spectrum” *Phys. Rev. D* **73**, 024009 (2006); arXiv:gr-qc/0509026.
- [17] A. López-Ortega, “Electromagnetic quasinormal modes of  $d$ -dimensional black holes”, *Gen. Relativ. Gravit.* **38**, 1747 (2006); arXiv:gr-qc/0605034.
- [18] A. Zhidenko, *Linear Perturbations of Black Holes: Stability, Quasinormal Modes and Tails*, (PhD thesis, IFUSP, Universidade de São Paulo, 2009); arXiv:0903.3555 [gr-qc].
- [19] J. G. Rosa and S. R. Dolan, “Massive vector fields on the Schwarzschild spacetime: Quasinormal modes and bound states”, *Phys. Rev. D* **85**, 044043 (2012); arXiv:1110.4494 [hep-th].

- [20] C. Herdeiro, M. O. P. Sampaio, and M. Wang, “Hawking radiation for a Proca field in  $d$ -dimensions”, *Phys. Rev. D* **85**, 024005 (2012); arXiv:1110.2485 [gr-qc].
- [21] P. Pani, “Advanced methods in black-hole perturbation theory”, *Int. J. Mod. Phys. A* **28**, 1340018 (2013); arXiv:1305.6759 [gr-qc].
- [22] S. R. Dolan, “Instability of the Proca field on Kerr spacetime”, *Phys. Rev. D* **98**, 104006 (2018); arXiv:1806.01604 [gr-qc].
- [23] J. Percival and S. R. Dolan, “Quasinormal modes of massive vector fields on the Kerr spacetime”, *Phys. Rev. D* **102**, 104055 (2020); arXiv:2008.10621 [gr-qc].
- [24] S. Garcia-Saenz, A. Held, and J. Zhang, “Schwarzschild quasinormal modes of non-minimally coupled vector fields”, *J. High Energy Phys. JHEP* **05** (2022) 139; arXiv:2202.07131 [gr-qc].
- [25] S. R. Dolan, M. A. A. de Paula, L. C. S. Leite, and L. C. B. Crispino, “Superradiant instability of a charged regular black hole”, *Phys. Rev. D* **109**, 124037 (2024); arXiv:2401.14967 [gr-qc].
- [26] F. Mellor and I. Moss, “Stability of black holes in de Sitter space”, *Phys. Rev. D* **41**, 403 (1990).
- [27] V. Cardoso and J. P. S. Lemos, “Quasinormal modes of the near extremal Schwarzschild-de Sitter black hole”, *Phys. Rev. D* **67**, 084020 (2003); arXiv:gr-qc/0301078.
- [28] A. Zhidenko, “Quasinormal modes of Schwarzschild-de Sitter black holes”, *Classical Quantum Gravity* **21**, 273 (2004); arXiv:gr-qc/0307012.
- [29] R. A. Konoplya and A. Zhidenko, “Nonoscillatory gravitational quasinormal modes and telling tails for Schwarzschild-de Sitter black holes”, *Phys. Rev. D* **106**, 124004 (2022); arXiv:2209.12058 [gr-qc].
- [30] R. A. Konoplya, “Two regimes of asymptotic fall-off of a massive scalar”, field in the Schwarzschild-de Sitter spacetime”, *Phys. Rev. D* **109**, 104018 (2024); arXiv:2401.17106 [gr-qc].
- [31] G. T. Horowitz and V. E. Hubeny, “Quasinormal modes of AdS black holes and the approach to thermal equilibrium”, *Phys. Rev. D* **62**, 024027 (2000); arXiv:hep-th/9909056.
- [32] V. Cardoso and J. P. S. Lemos, “Scalar, electromagnetic and Weyl perturbations of BTZ black holes: Quasinormal modes”, *Phys. Rev. D* **63**, 124015 (2001); arXiv:gr-qc/0101052 [gr-qc].
- [33] V. Cardoso and J. P. S. Lemos, “Quasinormal modes of Schwarzschild anti-de Sitter black holes: Electromagnetic and gravitational perturbations”, *Phys. Rev. D* **64**, 084017 (2001); arXiv:gr-qc/0105103.
- [34] V. Cardoso and J. P. S. Lemos, “Quasinormal modes of toroidal, cylindrical and planar black holes in anti-de Sitter spacetimes: Scalar, electromagnetic, and gravitational perturbations”, *Classical Quantum Gravity* **18**, 5257 (2001); arXiv:gr-qc/0107098.
- [35] E. Berti and K. D. Kokkotas, “Quasinormal modes of Reissner-Nordström-anti-de Sitter black holes: Scalar, electromagnetic, and gravitational perturbations”, *Phys. Rev. D* **67**, 064020 (2003); arXiv:gr-qc/0301052.
- [36] V. Cardoso, J. P. S. Lemos, and R. A. Konoplya, “Quasinormal frequencies of Schwarzschild black holes in anti-de Sitter spacetimes: A complete study on the asymptotic behavior”, *Phys. Rev. D* **68**, 044024 (2003); arXiv:gr-qc/0305037.
- [37] H. Kodama and A. Ishibashi, “A master equation for gravitational perturbations of maximally symmetric black holes in higher dimensions”, *Prog. Theor. Phys.* **110**, 701 (2003); arXiv:hep-th/0305147.
- [38] H. Kodama and A. Ishibashi, “Stability of higher-dimensional Schwarzschild black holes”, *Prog. Theor. Phys.* **110**, 901 (2003); arXiv:hep-th/0305185.
- [39] H. Kodama and A. Ishibashi, “Master equations for perturbations of generalised static black holes with charge in higher dimensions”, *Prog. Theor. Phys.* **111**, 24 (2004); arXiv:hep-th/0308128.
- [40] A. Ishibashi and R. M. Wald, “Dynamics in non-globally-hyperbolic static spacetimes : III. Anti-de Sitter spacetime”, *Classical Quantum Gravity* **21**, 2981 (2004); arXiv:hep-th/0402184.
- [41] A. S. Miranda and V. T. Zanchin, “Quasinormal modes of plane-symmetric anti-de Sitter black holes: A complete analysis of the gravitational perturbations”, *Phys. Rev. D* **73**, 064034 (2006); arXiv:gr-qc/0510066.
- [42] V. Cardoso, O. J. C. Dias, and S. Yoshida, “Classical instability of Kerr-AdS black holes and the issue of final state”, *Phys. Rev. D* **74**, 044008 (2006); arXiv:hep-th/0607162.
- [43] J. J. Friess, S. S. Gubser, G. Michalogiorgakis, and S. S. Pufu, “Expanding plasmas and quasinormal modes of anti-de Sitter black holes”, *J. High Energy Phys. JHEP* **04**, (2007) 080; arXiv:hep-th/0611005.
- [44] G. Siopsis, “Low frequency quasinormal modes of AdS black holes”, *J. High Energy Phys. JHEP* **05** (2007) 042; arXiv:hep-th/0702079.
- [45] R. A. Konoplya and A. Zhidenko, “Stability of higher dimensional Reissner-Nordström-anti-de Sitter black holes”, *Phys. Rev. D* **78**, 104017 (2008); arXiv:0809.2048 [hep-th].
- [46] E. Berti, V. Cardoso, and P. Pani, “Breit-Wigner resonances and the quasinormal modes of anti-de Sitter black holes”, *Phys. Rev. D* **79**, 101501 (2009); arXiv:0903.5311 [gr-qc].
- [47] M. Wang and C. Herdeiro, “Superradiant instabilities in a  $d$ -dimensional small Reissner-Nordström-anti-de Sitter black hole”, *Phys. Rev. D* **89**, 084062 (2014); arXiv:1403.5160 [gr-qc].
- [48] M. Wang, C. Herdeiro, and M. O. Sampaio, “Maxwell perturbations on asymptotically anti-de Sitter spacetimes: Generic boundary conditions and a new branch of quasinormal modes”, *Phys. Rev. D* **92**, 124006 (2015); arXiv:1510.04713 [gr-qc].
- [49] K. Ueda and A. Ishibashi, “Massive vector field perturbations on extremal and near-extremal static black holes”, *Phys. Rev. D* **97**, 124050 (2018); arXiv:1805.02479 [gr-qc].
- [50] T. V. Fernandes, D. Hilditch, J. P. S. Lemos, and V. Cardoso, “Quasinormal modes of Proca fields in a Schwarzschild-AdS spacetime”, *Phys. Rev. D* **105**, 044017 (2022); arXiv:2112.03282 [gr-qc].
- [51] T. V. Fernandes, D. Hilditch, J. P. S. Lemos, and V. Cardoso, “Normal modes of Proca fields in AdS spacetime”, *Gen. Relativ. Gravit.* **55**, 5 (2023); arXiv:2301.10248 [gr-qc].
- [52] K. Lin, “Quasinormal modes and echo effect of cylindrical anti-de Sitter black hole spacetime with a thin shell”, *Phys. Rev. D* **107**, 124002 (2023); arXiv:2306.01269 [gr-qc].
- [53] S. Kinoshita, T. Kozuka, K. Murata, and K. Sugawara, “Quasinormal mode spectrum of the AdS black hole with the Robin boundary condition”, *Classical Quantum*

- Gravity **41**, 055010 (2024); arXiv:2305.17942 [gr-qc].
- [54] D. Lopes, T. V. Fernandes, and J. P. S. Lemos, “Normal modes of Proca fields in  $\text{AdS}^d$  spacetime”, Phys. Rev. D **109**, 064041 (2024); arXiv:2401.13030 [gr-qc].
- [55] J. Barragán Amado, T. V. Fernandes, and D. C. Lopes “Quasinormal modes of a Proca field in Schwarzschild- $\text{AdS}_5$  spacetime via the isomonodromy method”, J. High Energy Phys. JHEP 09 (2025) 108; arXiv:2504.00080 [gr-qc].
- [56] J. P. S. Lemos, “A profusion of black holes from two to ten dimensions”, in *Proceedings of the XVIIth Brazilian Meeting of Particle Physics and Fields*, editor A. J. Silva (University of São Paulo Press, 1997), p. 40; arXiv:hep-th/9701121.
- [57] L. M. Sokółowski, “The bizarre anti-de Sitter spacetime”, Int. Jour. Geom. Meth. Mod. Phys. **13**, 1630016 (2016); arXiv:1611.01118 [gr-qc].
- [58] G. Bertone and D. Hooper, “A history of dark matter”, Rev. Mod. Phys. **90**, 45002 (2018); arXiv:1605.04909 [astro-ph.CO].
- [59] M. Abramowitz and I. A. Stegun, *Handbook of Mathematical Functions with Formulas, Graphs, and Mathematical Tables* (Dover, New York, 1965).